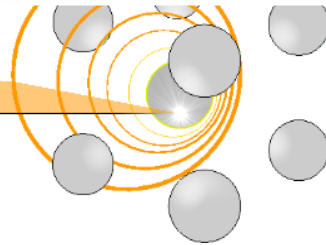


X-ray Absorption Spectroscopy investigations of disordered matter

Andrea Di Cicco

XAS LAB

X-ray Absorption Spectroscopy Laboratory - University of Camerino



School of Science and Technology

Physics Division

SiLS

SOCIETÀ ITALIANA LUCE DI SINCROTRONE
ITALIAN SYNCHROTRON RADIATION SOCIETY
www.synchrotron-radiation.it

Università di Camerino, Italy


XAFS 2018

17 International Conference
on X-Ray Absorption Fine Structure
22-27.07.2018 • Kraków • Poland

Camerino in 2009 and today



14th International Conference on X-ray Absorption Fine Structure
XAFS XIV Camerino 26 - 31 July 2009



Central Italy
earthquakes:
26 August 2016
(6.0), 26 Oct
2016(5.4,5.9), 30
Oct 2016 (6.5), 18
Jan 2017 (up to 5.5)
Situation slowly
normalizing ...



Di Cicco - Krakow XAFS conf. - Jul 2018

XAS group @Camerino

- Started in 1990
- <http://gnxas.unicam.it>



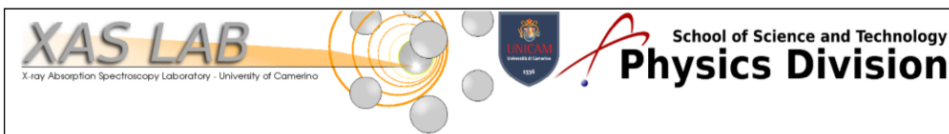
1992



1996

ukow XAFS conf. - Jul 2018

3



XAS group @ Camerino University

Principal Investigator: Prof. Andrea Di Cicco [MAIL](#) [HOME](#)

Researcher: Dr. Angela Trapananti [MAIL](#) [HOME](#)

Associate researcher: Dr. Marco Minicucci [MAIL](#) [HOME](#)

Post-doc researcher (with IOM/ICTP): Dr. S. J. Rezvani [MAIL](#) [HOME](#)

Students: [Matteo Ciambezi](#) [Emin Yimiti](#) - -

Affiliated groups @ Camerino University

Surface Science: Prof. Roberto Gunnella [MAIL](#) [HOME](#)

External Collaborators

Prof. Keisuke Hatada, Dr. F. Iesari (Univ. Toyama, Japan) [MAIL](#) [HOME](#)

Dr. Agnieszka Witkowska (Gdansk University of Technology) [MAIL](#) [HOME](#)

Prof. Adriano Filippini (University of L'Aquila) [MAIL](#) [HOME](#)

Dr. Giuliana Aquilanti ([ELETTRA XAFS beamline](#)) [MAIL](#) [HOME](#)

Dr. Simone De Panfilis ([IIT Sapienza](#)) [MAIL](#) [HOME](#)

Dr. Massimo Celino ([ENEA Casaccia](#)) [MAIL](#) [HOME](#)

Prof. Paola D'Angelo ([Università di Roma "La Sapienza"](#)) [MAIL](#) [HOME](#)

[HOME](#)

[RESEARCH](#)

[TEACHING](#)

[GNXAS](#)

[Publications and Highlights](#)

[Press and Awards](#)

[Life of the group](#)

[Links](#)



[Restricted area](#)

Summary

- XAS in disordered systems
- Overview on underlying theory and data-analysis
- Peak-fitting and RMC XAS structural refinements
- Validation and accuracy of structural results on typical examples (gas, crystals)
- Elemental liquids: open problems, experimental and sample environment issues (pressure/temperature)
- Selected results: liquids/undercooled at high temperature, liquids and amorphous systems under pressure
- A quick look into new experimental challenges

Why x-ray absorption in disordered matter?

- Typical systems:

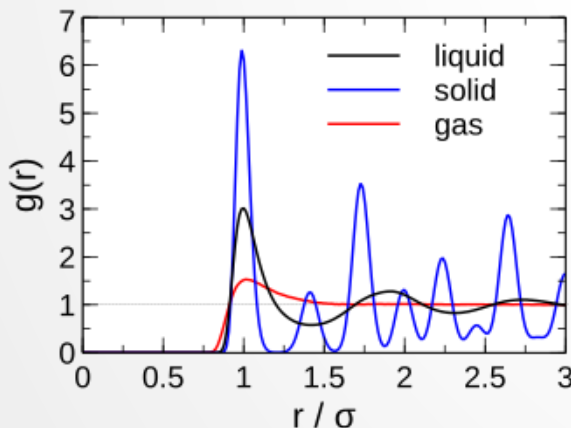
- 1) gases, liquids (thermodynamical equilibrium)
- 2) amorphous solids (including glasses, plastic/polymers, gels)
- 3) disordered thin films/ill-ordered nanostructures/alloys and composites

- Main advantages:

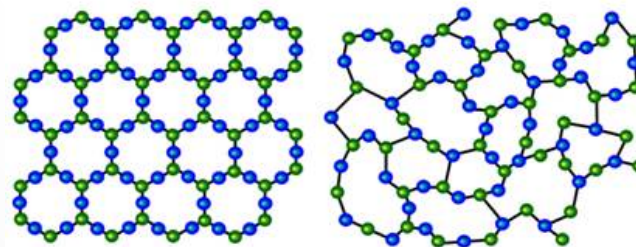
- 1) chemical selectivity
- 2) local probe, highly sensitive to short-range
- 3) experiments accessible under various sample environments
- 4) probing metastable and transient states

- Standard experimental techniques for structural studies include x-ray and neutron diffraction, as well as spectroscopies like Raman scattering

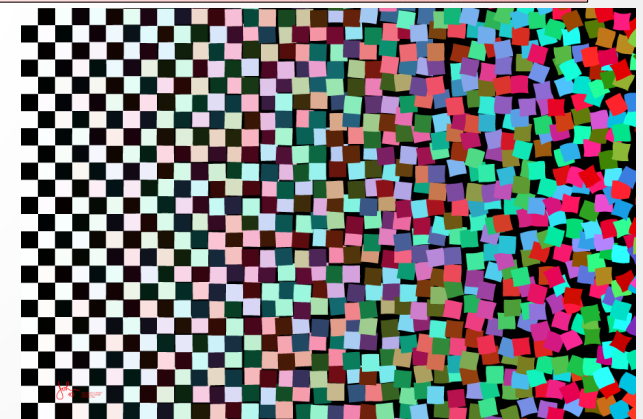
- XAS is powerful and highly complementary to the other techniques, but is blind to long-range correlations and needs complex data-analysis



Pair distribution function $g(r)\rho 4\pi r^2 dr = dn(r)$

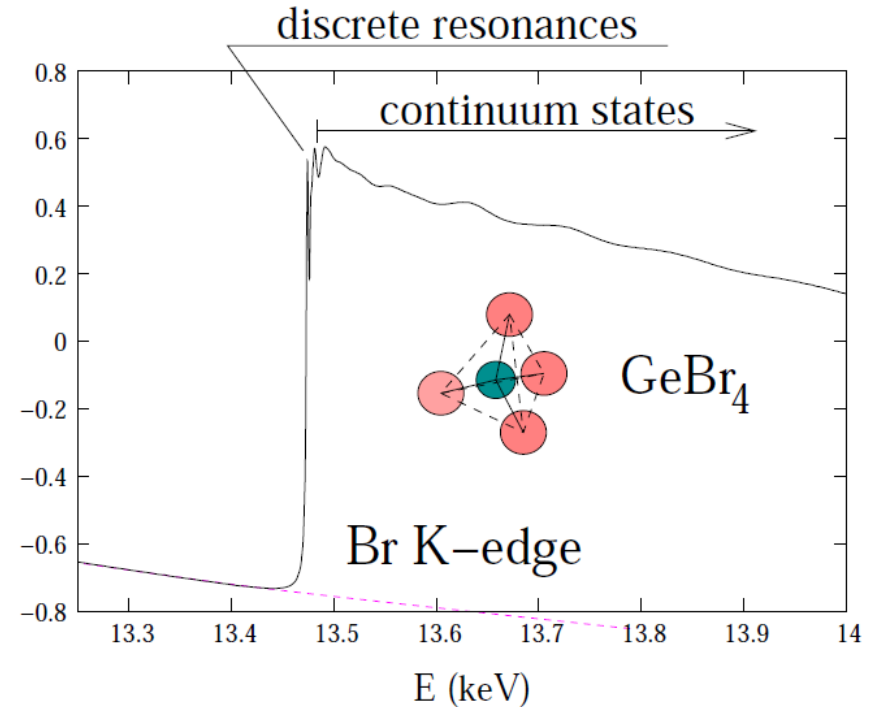


Courtesy www.bnc.hu



X-ray Absorption Spectroscopy

- The phenomenon of X-ray absorption is mainly associated with core electron excitations.
- The K, L ... threshold sequence suggests it is mostly a one-electron phenomenon.
- Relevant matrix element $\langle \Psi_i | \epsilon \cdot \hat{p} | \Psi_f \rangle$
- Typical transition times 10^{-15} s (instantaneous with respect to atomic motion).



- A probe for average properties around the selected photoabsorber atomic species:
 - unoccupied density of **electronic states** (projected + excitonic effect)
 - short-range structure** (partial radial distribution functions)
- Can be indifferently applied to **gas, liquid and solid** (amorphous or crystalline) phases
- Suitable for investigations under **extreme thermodynamic conditions** (HP-HT)
- Full bulk sensitivity: typical sample thickness 0.01–10 mm

Modeling x-ray absorption using the MS theory

The polarization averaged XAS cross-section for transitions to a dipole selected final state of angular momentum l_0 can be written as

$$(42) \quad \sigma(\omega) = \sigma_0 \left[\Im \frac{1}{\Im(t_0^{l_0})} \frac{1}{2l_0 + 1} \sum_{m_0} [T(I - GT)^{-1}]_{0,0}^{L_0, L_0} \right].$$

Here σ_0 is the atomic cross-section, T and G are the atomic scattering and propagator matrices in a local basis, indexed by i, j running over the different atoms, and by a set of angular momenta L, L' (where $L = \{l, m\}$).

The T scattering matrix here is block diagonal ($T_{i,j} = t_i \delta_{i,j}$) and, in the MT approximation for the potential, also diagonal on the the L indices ($t_i^{L,L'} = t_i^L \delta_{L,L'}$).

$$(43) \quad T = t_i \delta_{i,j} \delta_{l,l'} \delta_{m,m'}$$

In terms of the l -th potential phase shift: $t_i^l = \exp(i\delta_i^l) \sin(\delta_i^l)$.

T matrix elements are calculated by solving the Schrödinger equation for the potential at the corresponding i site.

Remark: all MS equations, and in particular the XAS cross-section, remains unaltered if one replaces the MT spheres with space filling cells (no interstitial region), but t^l is replaced by $t^{L,L'}$, taking in this way into account the non spherical shape of the cell potential (non MT potentials).

Geometry probed by propagators

The propagator matrix is composed of null diagonal blocks, (i, i) sites, and non null off-diagonal blocks $G_{i,j}^{L,L'}$ describing the free propagation from site i to site j ($i \neq j$). The expression for a single propagator block involves 3J symbols and is given by:

$$(44) \quad G_{i,j}^{L,L'} = [4\pi(2l+1)(2l'+1)]^{\frac{1}{2}} \sum_{l_1} (2l_1+1)^{\frac{1}{2}} \begin{pmatrix} l & l' & l_1 \\ 0 & 0 & 0 \end{pmatrix} \begin{pmatrix} l & l' & l_1 \\ m & -m' & m'-m \end{pmatrix} (-1)^{m'} i^{l_1+1} h_{l_1}^+(kR_{ij}) Y_{l_1, m'-m}(\hat{R}_{i,j}).$$

Here h_l^+ are Hankel functions, $Y_{l,m}$ are the spherical harmonics and $\vec{R}_{i,j}$ the vector joining site j to site i .

$$(45) \quad G_{i,j}^{L,L'} \neq 0 \text{ only if } i \neq j$$

Describe the site to site wave propagation.

$$\underline{h}_l^+(kr) \sim \frac{e^{ikr}}{kr} \text{ asymptotic behaviour for } kr \gg l$$

Chemistry – structure decoupling

The two important matrices appearing in the cross-section are related to the chemistry (T using only atom indexing):

$$(46) \quad T = \begin{pmatrix} t_0 & 0 & 0 & \dots & 0 \\ 0 & t_1 & 0 & \dots & 0 \\ \dots & \dots & \dots & \dots & \dots \\ 0 & 0 & \dots & t_{N-1} & 0 \\ 0 & 0 & \dots & 0 & t_N \end{pmatrix}$$

and to the geometry (G):

$$(47) \quad G = \begin{pmatrix} 0 & G_{0,1} & G_{0,2} & \dots & G_{0,N} \\ G_{1,0} & 0 & G_{2,0} & \dots & G_{1,N} \\ \dots & \dots & \dots & \dots & \dots \\ G_{N-1,0} & G_{N-1,1} & \dots & 0 & G_{N-1,N} \\ G_{N,0} & G_{N,1} & \dots & G_{N,N-1} & 0 \end{pmatrix}$$

Electron interaction and structure are decoupled! In this approach the model optical potential is included in the scattering matrices t_i (irrespective of their positions). Conversely, the matrices G_{ij} contain only information on the geometrical dispositions of atoms i and j irrespective of their actual scattering power.

Multiple-scattering expansion

- Non-linear relationship between geometry and XAS signal:

$$\sigma \sim (I - GT)^{-1}$$

Non linearity: mathematical consequence of the strong coupling of the photoelectron with the surrounding atoms (more difficulties in analyzing XAS data).

- First approach: multiple scattering (MS) expansion. Where the norm of the GT matrix (maximum modulus of its eigenvalues) satisfies $\|GT\| < 1$ then the formal matrix expansion $T(I - GT)^{-1} = T(I + GT + GTGT + GTGTGT + \dots)$ is convergent and gives rise to the MS series.

The above condition will certainly hold above a given energy since not only the elements of the G matrix decrease like $1/\sqrt{E}$ but also $\|T\| = \max |t_i|$ tends to zero much more rapidly with energy. The convergence threshold is system dependent, typical values range from below the edge to a few Ry.

- Writing down the series we obtain:

$$(48) \quad \sigma(\omega) = \sigma_0 \left[1 + \sum_{i \neq 0} \chi_2^{0i0} + \sum_{\substack{i \neq j \\ i \neq 0, j \neq 0}} \chi_3^{0ij0} + \sum_{\substack{i \neq j \neq k \\ i \neq 0, k \neq 0}} \chi_4^{0ijk0} + \dots \right]$$

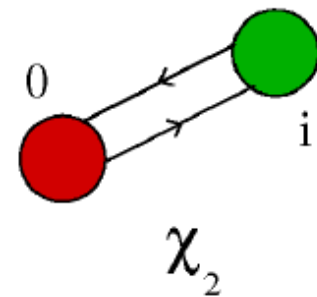
Multiple-scattering signals

The generic χ_n structural term is:

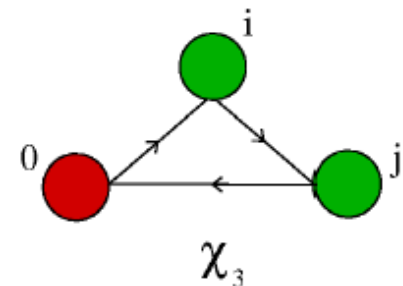
$$(49) \quad \chi_n^{0i\dots j0} = \mathfrak{S} \left(\frac{t_0^{l_0}}{\mathfrak{S}(t_0^{l_0})} \frac{1}{2l_0 + 1} \sum_{m_0} (\Xi^{0i\dots j0})_{L_0, L_0} \right)$$

and specifically $\Xi^{0i0} = G_{0,i}t_i G_{i,0}t_0$ for χ_2^{0i0} , $\Xi^{0ij0} = G_{0,j}t_j G_{j,i}t_i G_{i,0}t_0$ for χ_3^{0ij0} , and $\Xi^{0ijk0} = G_{0,k}t_k G_{k,j}t_j G_{j,i}t_i G_{i,0}t_0$ for χ_4^{0ijk0} . In this notation it is understood that the internal angular momentum indices have been saturated.

$$(50) \quad \chi_2^{0i0} = \mathfrak{S} \left(\frac{t_0^{l_0}}{\sin^2(\delta_0^{l_0})} \frac{1}{2l_0 + 1} \sum_{m_0} (G_{0,i}t_i G_{i,0}t_0)_{L_0, L_0} \right)$$



$$(51) \quad \chi_3^{0ij0} = \mathfrak{S} \left(\frac{t_0^{l_0}}{\sin^2(\delta_0^{l_0})} \frac{1}{2l_0 + 1} \sum_{m_0} (G_{0,j}t_j G_{j,i}t_i G_{i,0}t_0)_{L_0, L_0} \right)$$



The XAS n-body expansion (GnXAS)

- On the other hand, the total cross-section for n atoms $\sigma(0, i, j \dots n)$ can be expanded in terms of the irreducible n -body cross sections of lower order. A useful expansion is thus obtained:

$$(5) \quad \sigma(0, i, j \dots, n) = \sigma_0 + \sum_i \sigma^{(2)}(0, i) + \sum_{(i,j)} \sigma^{(3)}(0, i, j) + \\ + \sum_{(i,j,k)} \sigma^{(4)}(0, i, j, k) + \dots + \sigma^{(n)}(0, i, j, \dots, n).$$

- The dimensionless quantities $\gamma^{(n)} = \sigma^{(n)} / \sigma_0$, represent the irreducible n -body contributions to the structural XAS term $\chi(\omega) = \frac{\sigma(\omega) - \sigma_0}{\sigma_0}$ and we arrive to an equivalent expansion for the dimensionless experimental structural signal χ that differs substantially from the MS series:

$$(6) \quad \chi(0, i, j \dots, n) = \sum_i \gamma^{(2)}(0, i) + \sum_{(i,j)} \gamma^{(3)}(0, i, j) + \\ + \sum_{(i,j,k)} \gamma^{(4)}(0, i, j, k) + \dots + \gamma^{(n)}(0, i, j, \dots, n).$$

Original refs.: Phys. Rev. B 52, 15122 and 15135 (1995)

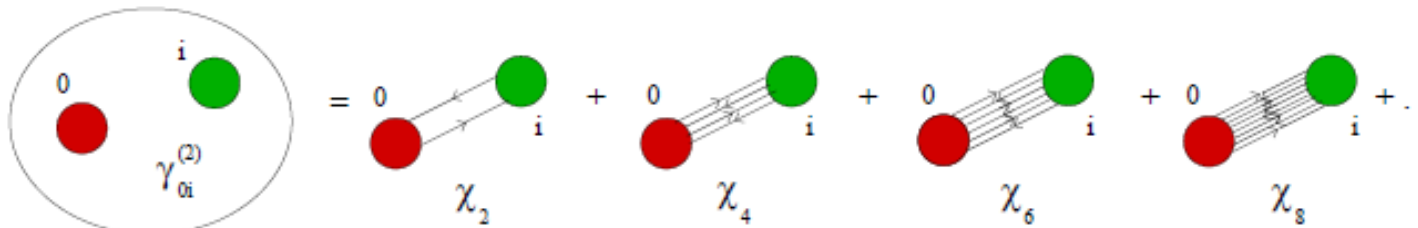
Irreducible n-body XAS signals

The irreducible n -body $\gamma^{(n)}$ signals are the central quantities in our approach, since they are associated with well precise n -body arrangements of the atoms.

- A simple linear relationship between structure (expressed in terms of 2, 3, 4, ... n -body distributions) and signal is obtained. The relationship contains a finite number of terms if the system is finite (cluster).
- Due to mean free path effects, the higher order n -body terms are generally smaller than the lower order ones, so that convergence with few terms is expected.
- Low-order $\gamma^{(n)}$ signals can be easily calculated with different methods (within GNXAS).

The corresponding MS expansion, pictorially depicted below, results:

$$(10) \quad \gamma^{(2)}(0, i) = \chi_2^{0i0} + \chi_4^{0i0i0} + \chi_6^{0i0i0i0} + \chi_8^{0i0i0i0i0} + \dots$$



XAS relationship with atom distribution

Having defined the irreducible $\gamma^{(n)}$ MS signals, the general expression of the XAS structural term is given in terms of the n -body distribution functions $g_n(r)$ (r is a generic set of n -body coordinates):

$$\begin{aligned}
 \langle \chi(k) \rangle = & \int_0^\infty dr 4\pi r^2 \rho g_2(r) \gamma^{(2)}(r, k) + \int dr_1 dr_2 d\phi 8\pi^2 r_1^2 r_2^2 \sin(\phi) \rho^2 g_3(r_1, r_2, \phi) \\
 & \times \gamma^{(3)}(r_1, r_2, \phi, k) + \int dr_1 dr_2 d\phi dr_3 d\Omega 8\pi^2 r_1^2 r_2^2 r_3^2 \sin(\phi) \rho^3 g_4(r_1, r_2, \phi, r_3, \Omega) \\
 (19) \quad & \times \gamma^{(4)}(r_1, r_2, \phi, r_3, \Omega, k) \cdots \cdots
 \end{aligned}$$

The integrals, because of the short range nature of the Kernels $\gamma^{(n)}$, are actually limited to a region of linear dimensions of the order of few Å. This is due to the strong electron interaction (mean free path).

This equation should be compared with the well known expression for the static structure factor (disordered system) which can be measured by using x-ray or neutron diffraction:

$$(20) \quad S(k) = 1 + \frac{4\pi\rho}{k} \int_0^\infty (g_2(r) - 1) r \sin(kr) dr.$$

The different nature of the Kernels, however, makes the structural information on the $g_2(r)$ obtainable in the two cases largely complementary (short vs. medium range information). Moreover, XAS can give information beyond the pair distribution!

For crystals, where diffraction gives obviously a richer information about atomic positions, XAS provides unique data about local correlated vibrations.

XAS structural refinement strategy

- The non-linear minimization is performed using the raw absorption data $\alpha(E_i)$ including noise (not the $\chi(k)$ or filtered data). The model absorption spectrum $\alpha_m(E_i)$ thus include background modelling:

$$(32) \quad \alpha_m(E_i) = \alpha_{bkg}(E_i) + \alpha_{exc}(E_i) + [1 + \chi_m(E_i)] \alpha_0(E_i)$$

where

$\alpha_0(E_i) = J\sigma_0(E_i)$ is the atomic absorption coefficient

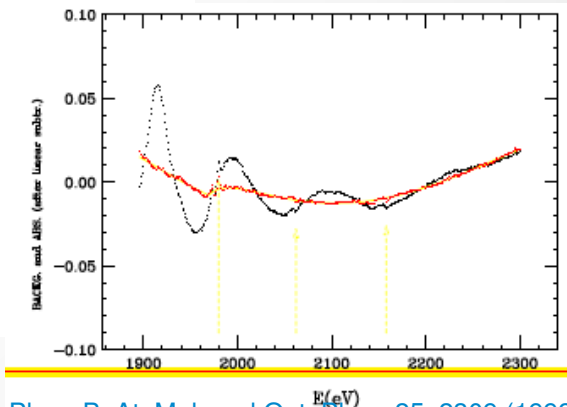
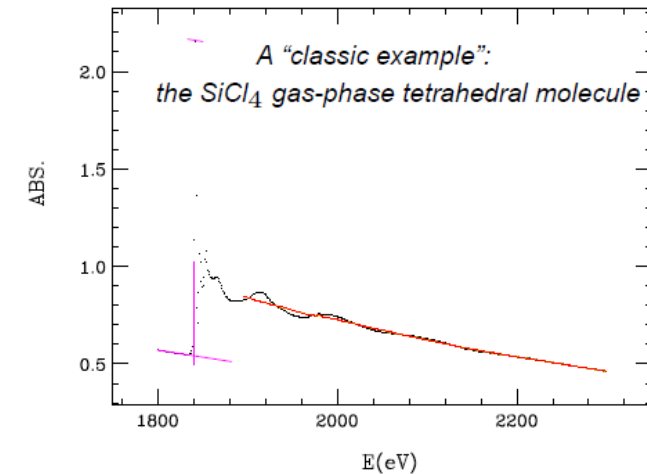
$\alpha_{bkg}(E_i)$ is a smooth polynomial background

$\alpha_{exc}(E_i)$ accounts for multi-electron excitation channels

- Simultaneous modelling of background and signal ($\chi_m(E_i)$) significantly reduces the introduction of systematic errors in the interpretation of the structural signal. Same approach for multi-edge studies:

$$(33) \quad \alpha_m(E_i) = \alpha_{bkg}(E_i) + \alpha_{exc}(E_i) + \sum_{j=1}^{NXAS} [1 + \chi_m^j(E_i)] \alpha_0^j(E_i)$$

Phys. Rev. B 53, 6174 (1996), Phys. Rev. B, 62, 12001 (2000)



J. Phys. B, At. Mol. and Opt. Phys. 25, 2309 (1992)

Background: multi-electron excitations

- *Multi-electron excitation channels: contribution may be of the order of 1% of the single-electron (main) channel. Realistic calculations of those channels are extremely difficult, only energy onsets can be reproduced accurately.*
- *Various model functions have been tested and used (within GNXAS). Inclusion is necessary to get quantitative agreement with the data.*
- *Multielectron excitations were studied in a variety of cases (3rd to 6th period Elements) also using photoemission spectroscopy.*
- *Very important for disordered systems (weaker XAS signal).*

AgBr (solid and liquid)

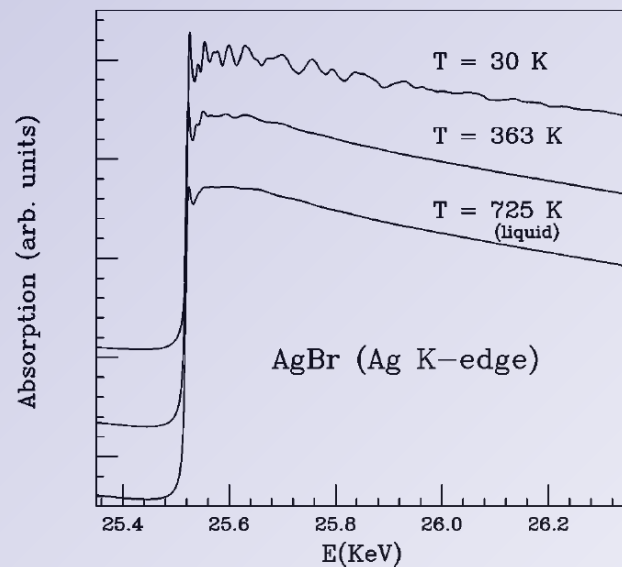
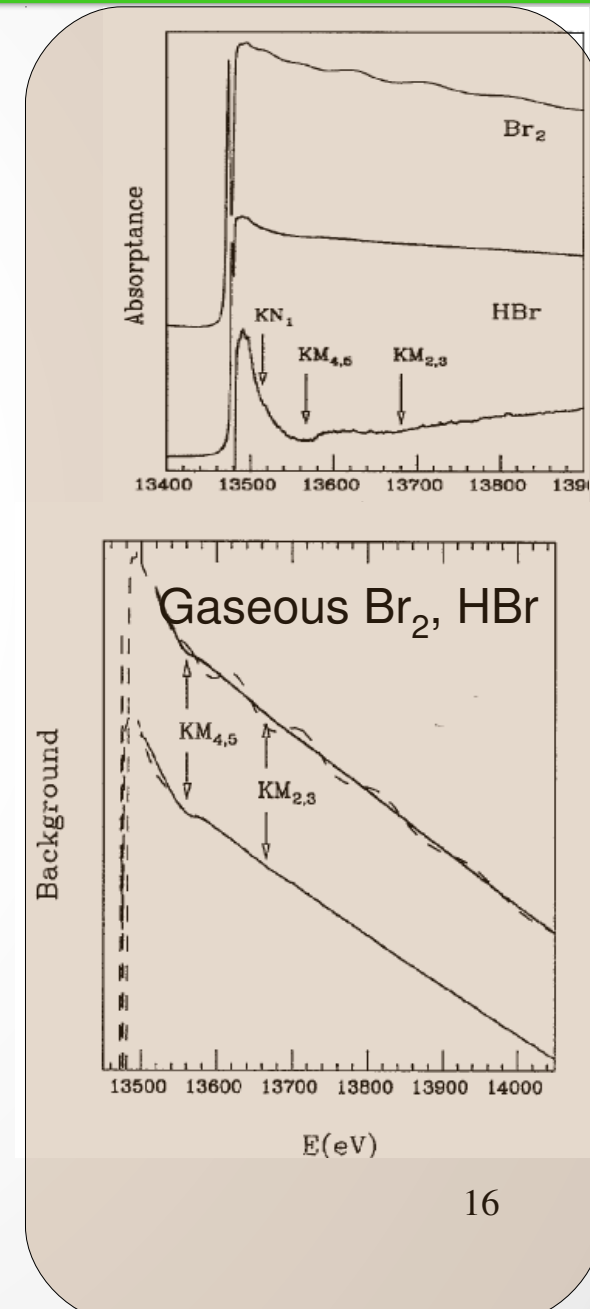
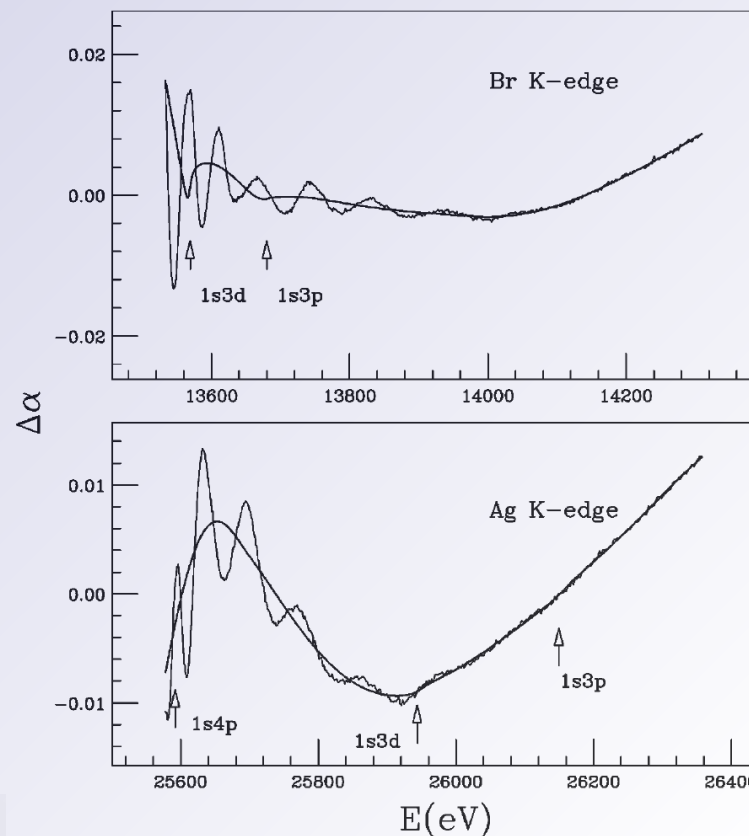


FIG. 3. X-ray absorption spectra of AgBr near the Ag K-edge are shown for three different temperatures in the solid and liquid phases.

Phys. Rev. B, 62, 12001 (2000)



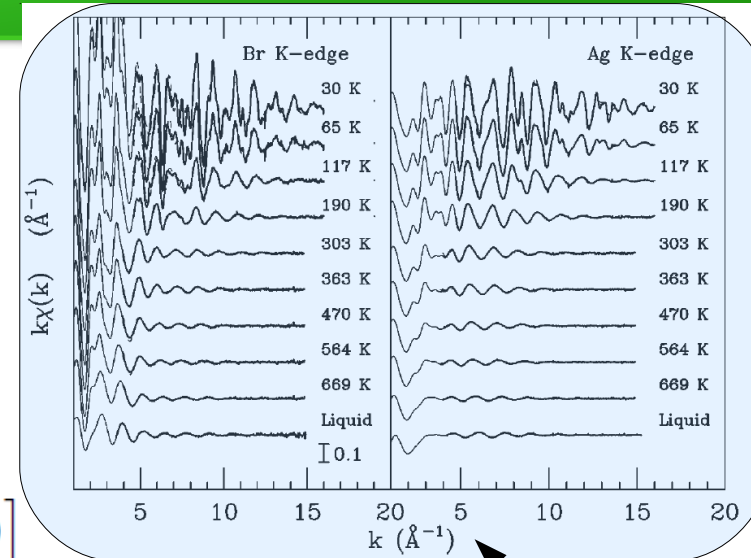
XAS structure refinement

The experimental structural signal is thus defined as:

$$(34) \quad \chi(E_i) = \frac{[\alpha(E_i) - \alpha_{bkg}(E_i) - \alpha_{exc}(E_i)]}{\alpha_0(E_i)}$$

or for multi-edge

$$(35) \quad \chi(E_i, j) = \frac{[\alpha(E_i) - \alpha_{bkg}(E_i) - \alpha_{exc}(E_i) - \sum_{l \neq j} J_l \sigma_{nor}(E_i, l) \chi(E_i, l)]}{\sigma_{nor}(E_i, j) \times J_j}$$



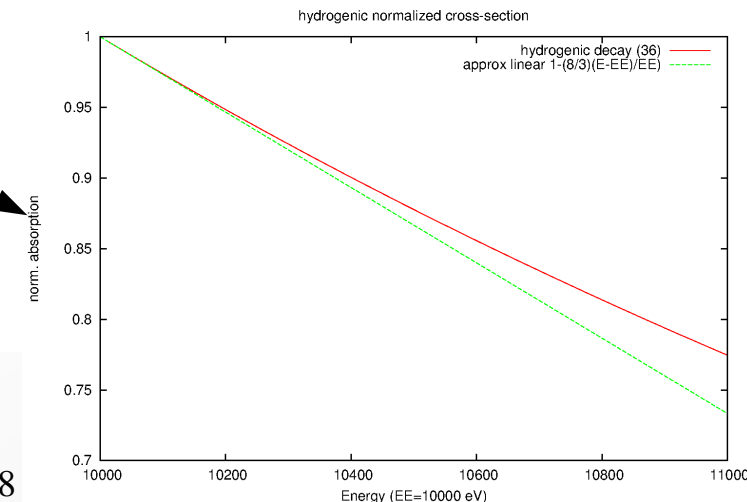
Phys. Rev. B 53, 6174 (1996), Phys. Rev. B, 62, 12001 (2000)

AgBr for
Increasing temperature

Normalization to the atomic cross-section is performed using a standard hydrogen-like absorption function $\sigma_{nor}(E_i)$, $\sigma_{nor}(E_i) \times J = \alpha_0(E_i)$:

$$(36) \quad \sigma_{nor}(E_i) = \frac{1}{e^{-4}} e^{(-4 \times \arctan \frac{1}{\eta})} \times \frac{1}{\left(1 + \frac{1}{\eta^2}\right)^4} \times \frac{1}{1 - e^{-2\pi\eta}}$$

where $\eta^2 = \frac{EE}{(E_i - EE)}$. Lengeler and P. Eisenberger, Phys. Rev. B 21, 4507 (1980)



Phys. Rev. B 52, 15135 (1995) -see refs. therein

Refinement procedures

- The function R which is minimized in the program is the sum over $i = 1, N$ points of the squares of the differences between model and experimental signals in the specified energy interval times a weight function:

$$(37) \quad R = \sum_i [\alpha(E_i) - \alpha_m(E_i, \{\lambda\})]^2 \times W(E_i)$$

Here the model signal $\alpha_m(i)$ depends on the ensemble of structural parameters $\{\lambda\}$. The weighting function $W(E_i)$ is calculated as:

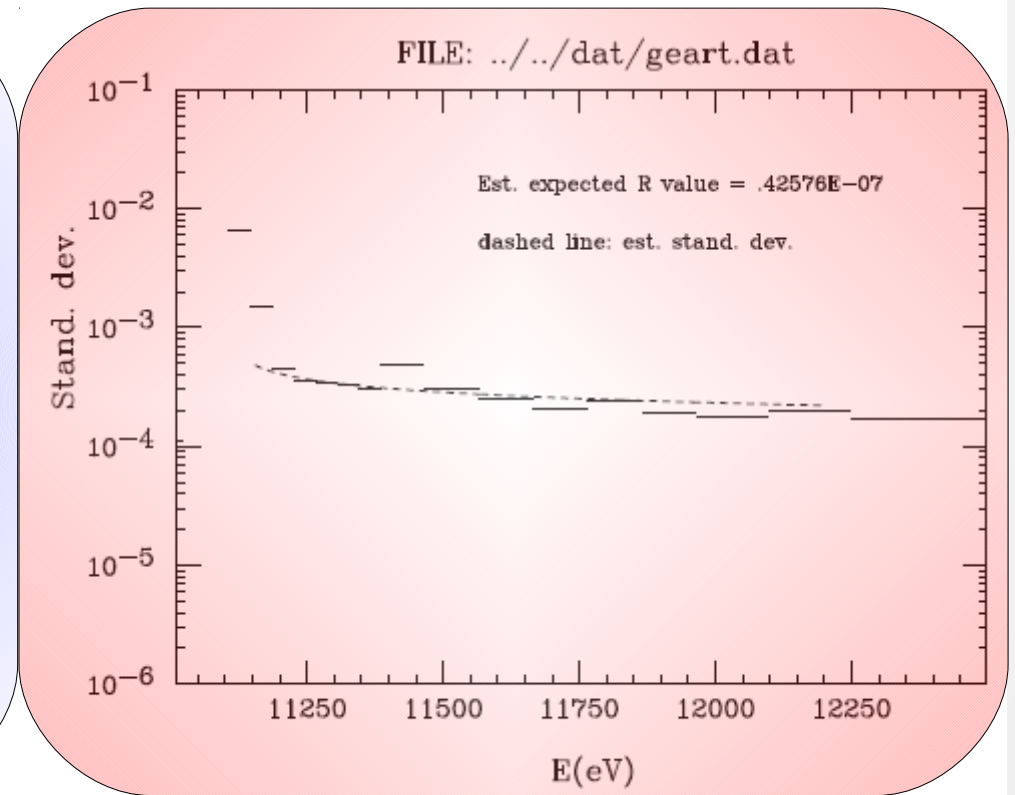
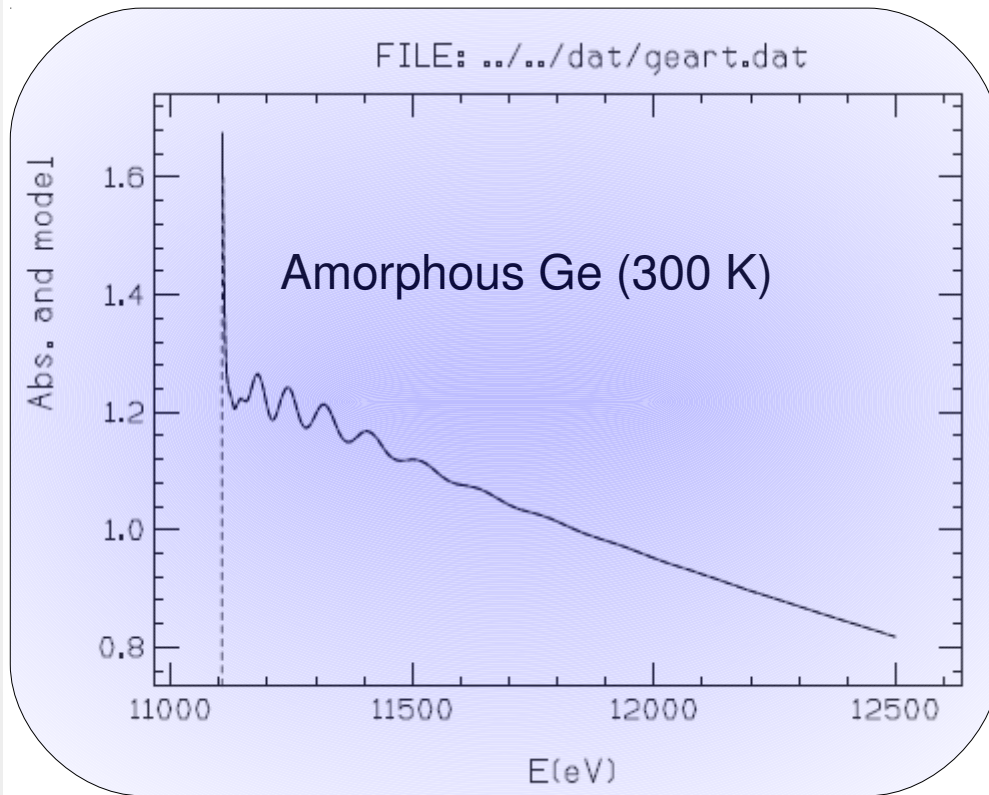
$$W(E_j) = \frac{N}{N - p} \times \frac{k_j^w}{\sum_i [\alpha_N(E_i)^2] \times k_i^w}$$

where $k_i (\text{\AA}^{-1}) \sim 0.512\sqrt{(E_i - EE)(\text{eV})}$ and p is the number of parameters used in the minimization. $\alpha_N(E_i) = \alpha(E_i) - a - b \times E_i$ is the absorption spectrum obtained removing the pre-edge linear background.

- Under normal conditions the weighting function should mimic the energy dependence of the inverse noise variance $1/\sigma_i^2$, so that the R function becomes a standard χ^2 like statistical function. This can be achieved by tuning the w (usually 1 – 4) parameter until a satisfactory agreement with the estimated noise is obtained, as can be verified graphically.

Statistical analysis: noise

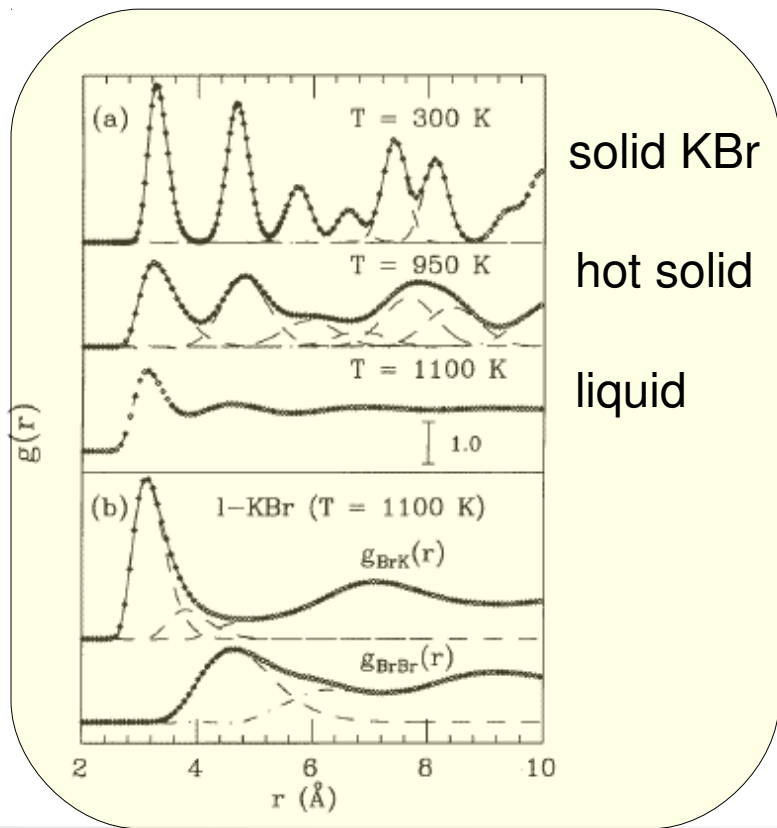
- Larger w values have the effect of giving a larger weight to higher energy data, and this choice can be adopted to reduce the weight of low energy data where the theoretical model may be less accurate.
- The expected value for the residual function R represents a weighted average squared noise (usually in the range 10^{-06} – 10^{-08}). In most of the real situations the actual minimum value of the residual will exceed these limiting values due to the presence of unexplained signal contributions.



Peak-fitting of the pair distribution

Structural refinement of the raw data through MS calculation of the XAS cross section (GNXAS $\rightarrow \gamma^{(n)}$ signals, corresponding to $g^{(n)}$ distributions)

- the distance distribution is assumed to be a superposition of distinct peaks (“shells”) whose parameters (N, R, σ^2, \dots) are fitted to the experimental data
- valid also for reconstructing the $g(r)$ in simple [1] and binary [2] liquids introducing physical constraints accounting for the density and the compressibility of the system



Needs:

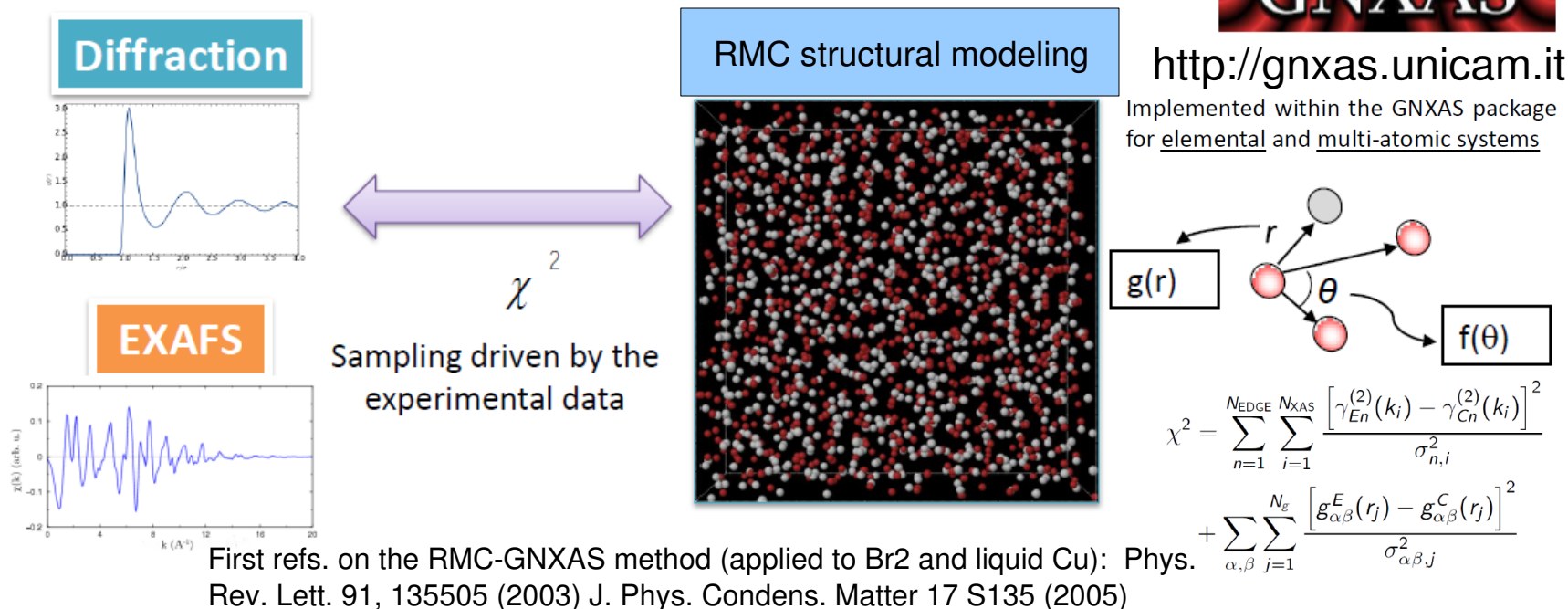
- Extension of the refinement scheme to multi-component systems and higher-order distributions
- Model independent approach
- Simultaneous refinement of short and long-range order (XAS+diffraction)

[1] A. Filipponi, Journal of Physics: CM 13, R23 (2001)
[2] Angela Trapananti and Andrea Di Cicco
Phys. Rev. B 70, 014101 (2004) <http://gnxas.unicam.it>

Beyond the peak-fitting approach

Data analysis: Reverse Monte Carlo

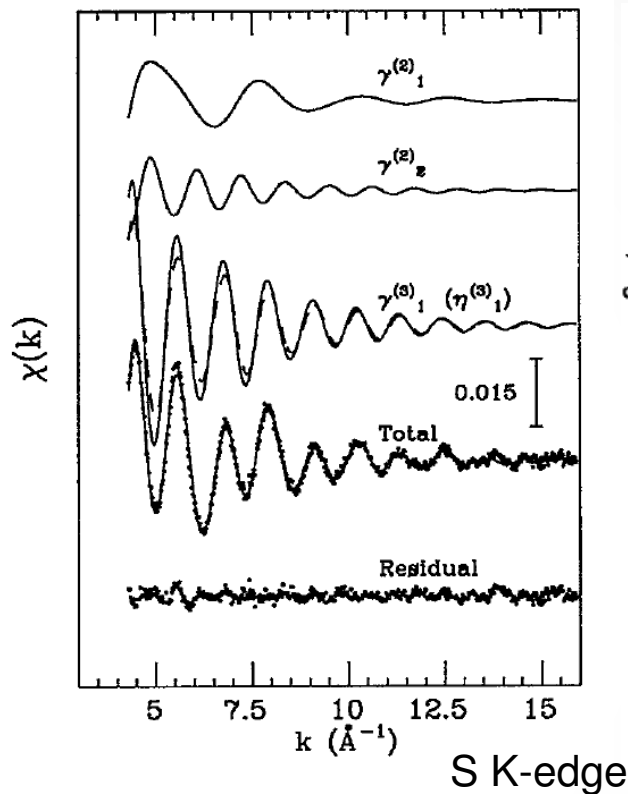
RMC is structural modelling approach to produce three dimensional atomic models of disordered materials which are consistent with a set of experimental data



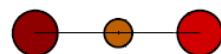
- RMC fully exploits the complementarity of different techniques
- 3d models: structural information beyond the average distance

Accuracy of XAS structure refinements: molecules

- Single and multiple-edge XAS refinements of gas-phase systems (using MS simulations and peak-fitting) have been shown to provide an accurate tool for measuring the distance (and angle) distributions
- Results have been found to be *in agreement* with electron diffraction data
- *Accuracy* in average distance determination can easily reach 0.002 Ang.
- *New information* on bond and angle distributions can be obtained

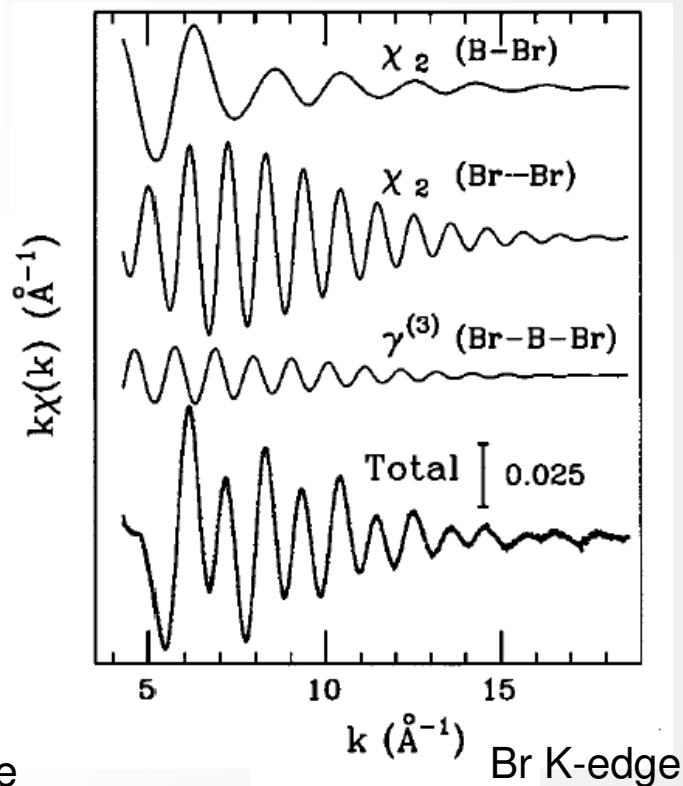


CS₂

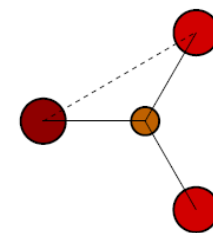


(linear)

Phys. Rev. B 52, 15122 (1995)



BBr₃



(planar)

Journal of Chemical Physics 109, 5356 (1998)

Accuracy of RMC-XAS structure refinements

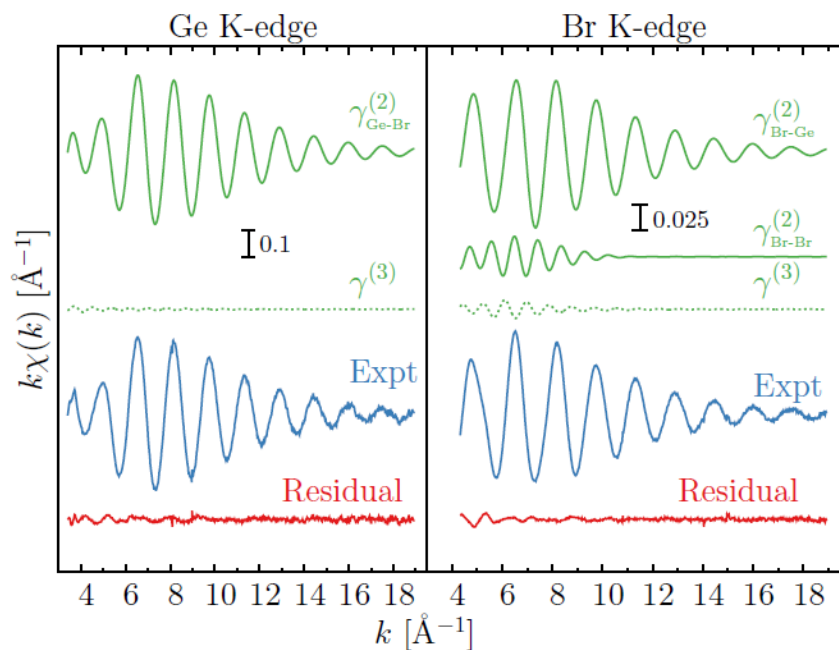
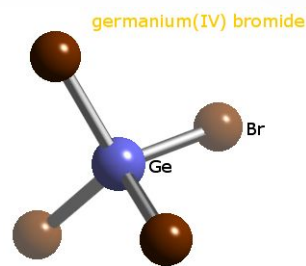
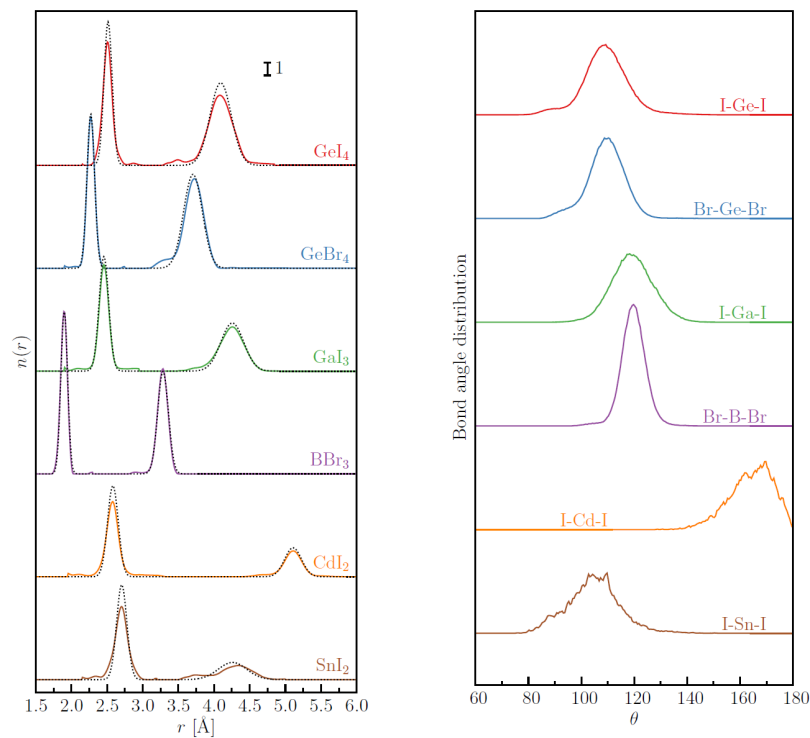


Figure 6. Double-edge RMC refinement of the Ge (left) and Br (right) K-edge EXAFS spectra of the GeBr_4 gas-phase system (temperature $T=403$ K). The calculated two-atom EXAFS signals resulting from a set of molecular configurations (green lines) are compared with the corresponding experimental data (blue lines). The weak three-body (γ^3) signals associated with the Br-Ge-Br triplet configurations are also shown. The residual curves are shown in red color (bottom).



Multiple-edge XAS refinements provide reliable determination of the short-range structure in molecules and condensed matter (using RMC and peak-fitting techniques)



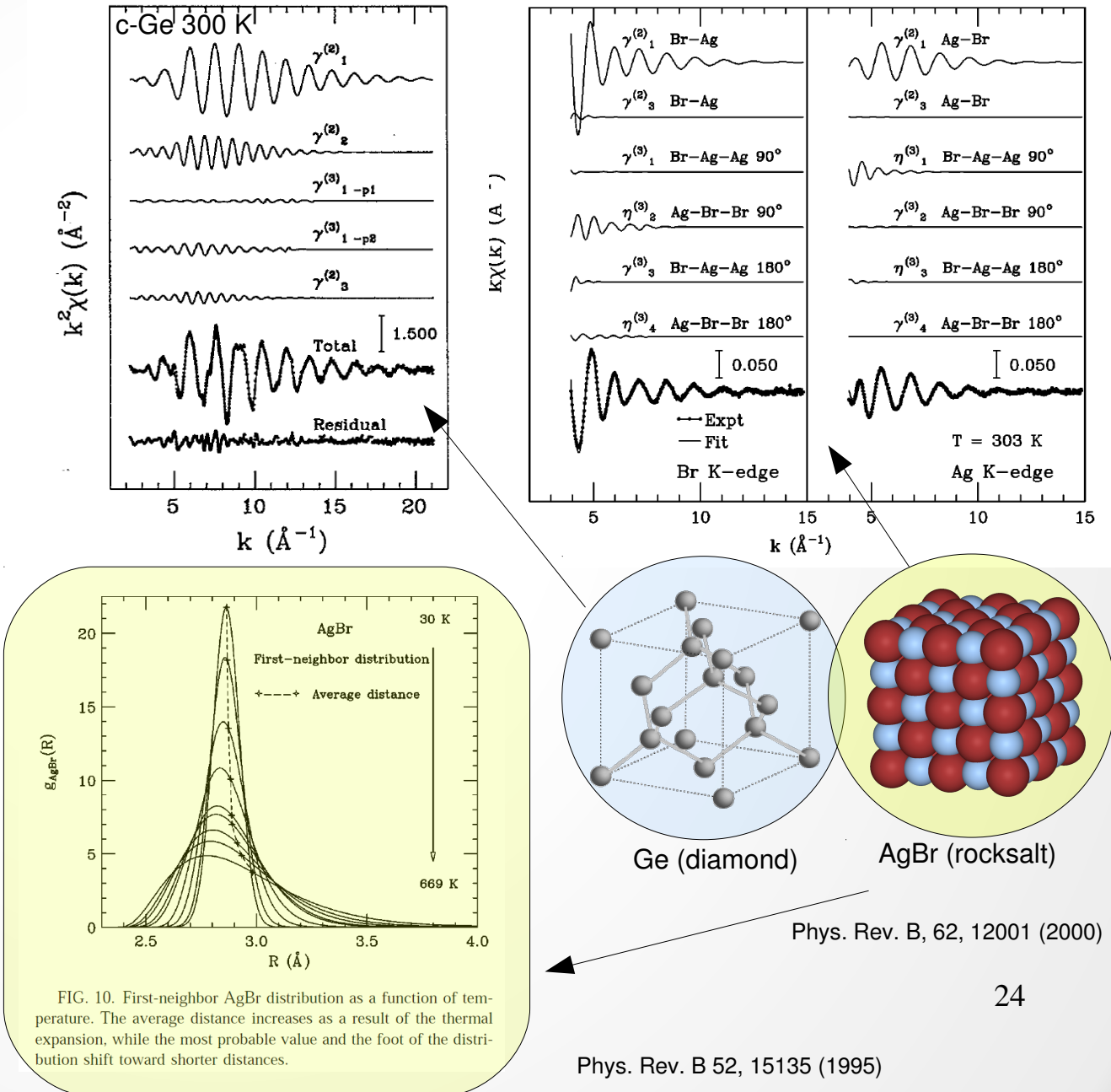
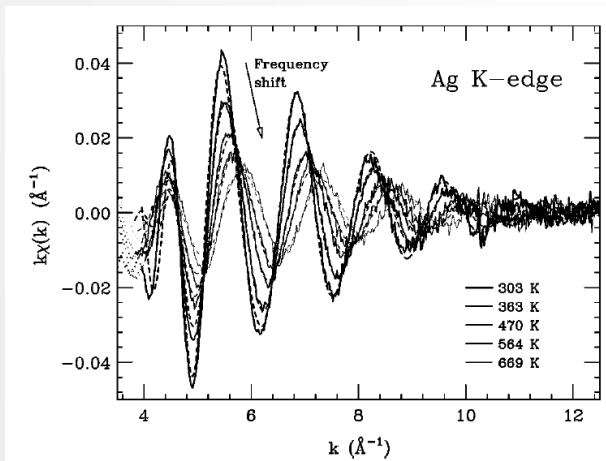
A. Di Cicco et al., J. Chem. Phys. 148, 094307 (2018)

Di Cicco - Krakow XAFS conf. - Jul 2018

Accuracy of XAS structure refinements: crystals

XAS refinements of simple crystalline systems (using MS simulations and peak-fitting) can probe the short-range distribution accurately

- Structural results can enrich the information obtained by XRD/ND.
 - Access to correlated vibrations (related to the phonon density of states)
- XAS provides direct and unique information about the deviation from the harmonic approximation (gaussian distribution of distances)



Elemental liquids

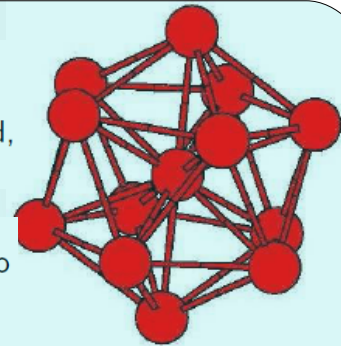
- Elemental liquids represent the simplest example of condensed disordered system under thermodynamical equilibrium.
- Measuring XAS of elemental liquids require solutions for sample design and high temperature conditions (with some notable exceptions like liquid Hg, Ga)
- Advances in experimental techniques allowed us to obtain accurate XAS measurements under controlled high-pressure and temperature conditions
- Phase transitions can be continuously monitored by a combination of techniques
- XAS has unique capabilities for measuring local structure of deeply undercooled liquids

Examples of open problems:

- Icosahedral ordering in close-packed liquids
- Poly(a)morphism of the liquid → existence of liquid-liquid transitions

The old hypothesis [F. C. Frank, Proc. R. Soc. London, Ser. A 215, 43 (1952)] that close packed liquids may develop an icosahedral order, especially when undercooled, has attracted attention for over half a century.

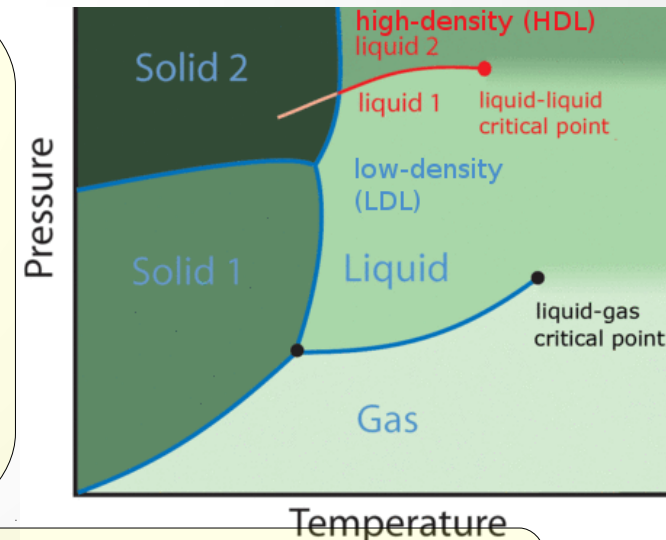
We contributed with a series XAS investigations of undercooled liquid elemental metals (Pd, Cu, Sn, Ni, ...) also addressing the issue of the degree of icosahedral local order developing in the melt.



>Polymorphic substances may show transitions also in their disordered phases (glass, undercooled liquid, liquid)

>This phenomenon is known to occur for amorphous ice under pressure, and has been suggested in other open-structure amorphous (or deeply undercooled) systems (low-density tetrahedral C, Si, Ge ..)

>Indications for liquid-liquid transitions in polymorphic metals (for example Sn, Bi) were also obtained by different techniques.



>Our XAS investigations regarded the occurrence of transitions in the Sn, Bi (undercooled) liquids under pressure, as well as in amorphous Ge and chalcogenides

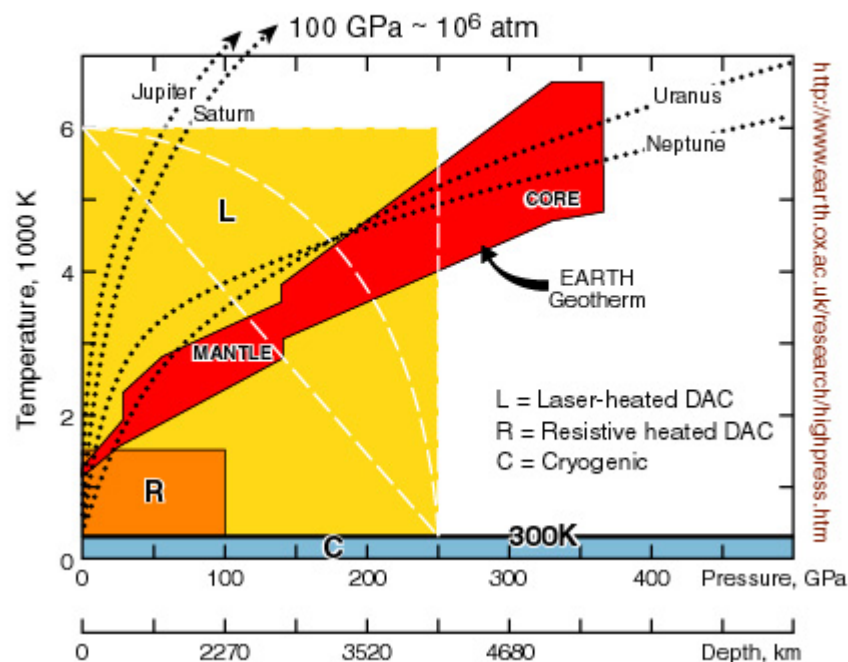
XAS of disordered systems under extreme (static) conditions

→ Recent advances in data-analysis and instrumentation allowed us to perform x-ray absorption (XAS) studies of liquids, undercooled liquids and glasses under high-temperature and/or high-pressure conditions. Interest for physics, geo-science and material science.

→ XAS and single-energy x-ray absorption, combined with x-ray diffraction, gives information about structure and transitions.

Advances in XAS data-analysis (using GNXAS/RMC) allowed detailed structural insight about pair and higher-order distributions. Recent applications to disordered matter include liquid and undercooled liquid metals like Cu, Ni, Pd, Ga, Pb, Ag, Sn, In, Bi, molten salts, aqueous solutions and metal alloys, as well as amorphous systems like a-Ge and glasses like GeSe_2 and As_2Se_3 .

ACCESSIBLE REGIONS OF P and T
(Modified from Mao & Hemley, Rev. Min. 37, 1998)



XAS/XRD experiments at high temperature

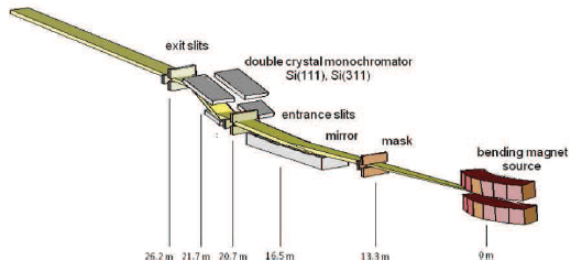


Figure 1. The basic optical concept of the XAFS beamline at ELETTRA. The mask define the size of the beam upstream the mirror. This one collimates the beam vertically before the double crystal monochromator in order to obtain the intrinsic energy resolution.

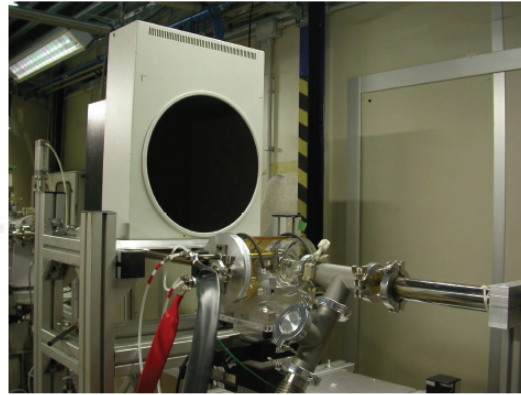


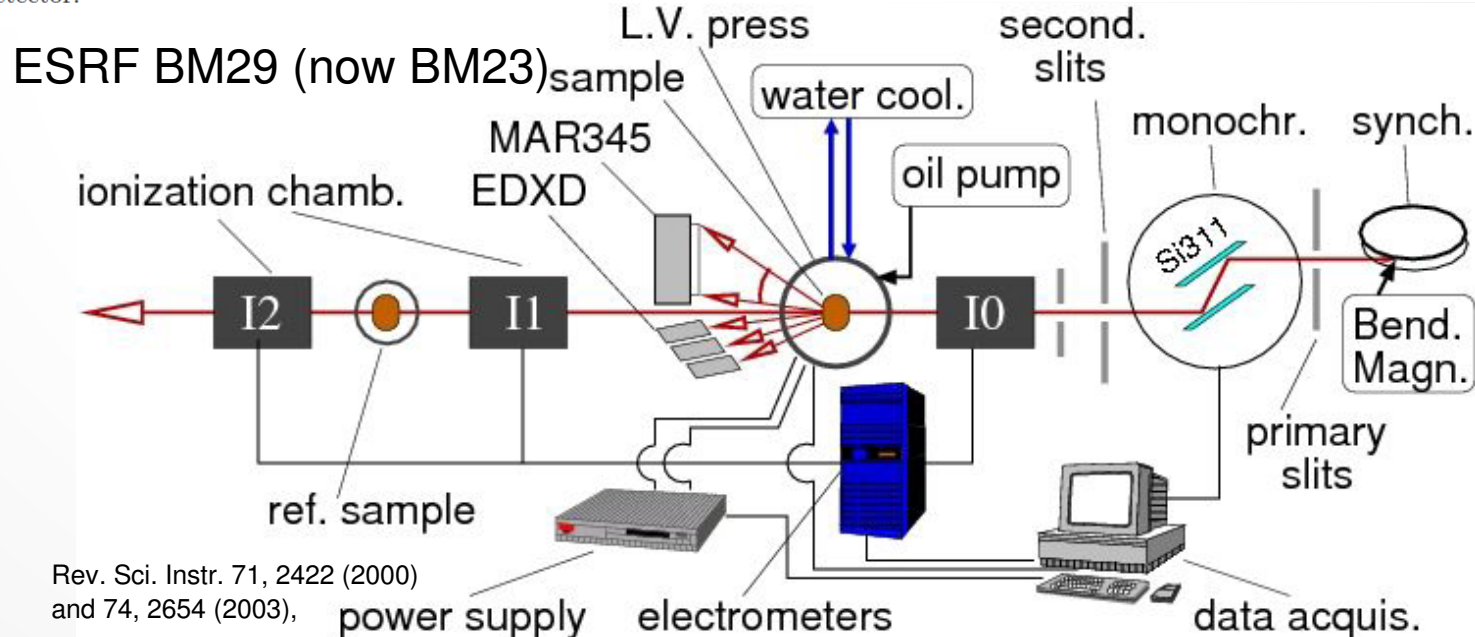
Figure 2. The high temperature L'Aquila-Camerino glass furnace for combined x-ray absorption and diffraction (custom version installed at XAFS@ELETTRA) and the vertical configuration for MAR image-plate detector.



Nucl. Inst. & Methods in Phys. Res. B 93, 302 (1994)

- - Wide temperature interval: 300 ÷ 2500 K
- - Clean high-vacuum ($\sim 10^{-5}$ mbar) sample environment
- - XAS/XRD measurements

Our high temperature XAS experiments began in Frascati (ADONE), late 80s and then suitable setups for the furnace were used at LURE (Orsay), ESRF and Elettra (since 2009). Simultaneous XRD/XAS spectra can be collected up to about 2500 K and more.

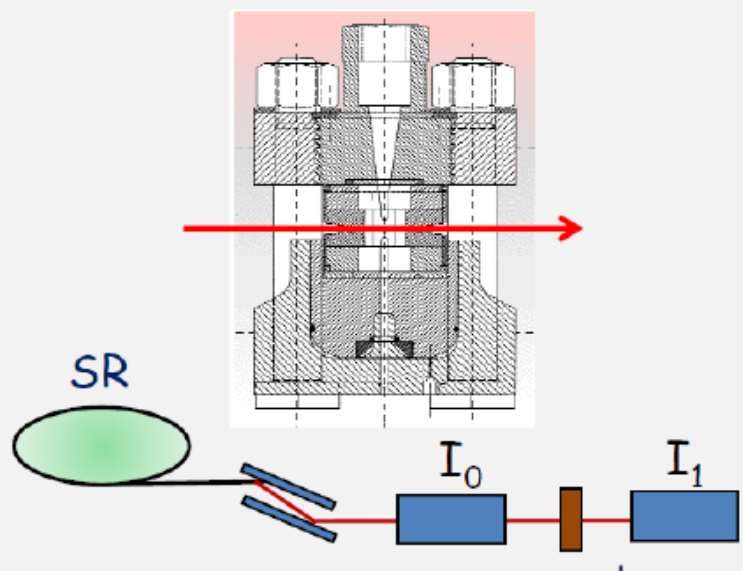


Rev. Sci. Instr. 71, 2422 (2000)
and 74, 2654 (2003),

Hardware for combined XAS-XRD-TSCAN experiments at HT-HP

Typical techniques for XAS at high (static) pressure

Paris-Edinburgh "large-volume"



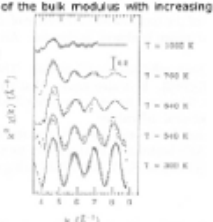
J. Phys. IV France **7** (1997) C2-1011-C2-1012
DOI: 10.1051/jp4:19972120

High-Pressure High-Temperature XAFS Investigation on HgTe

Y. Katayama¹, M. Mezouar², J.P. Itié², J.M. Besson², G. Syfousse², P. Le Fèvre⁴ and A. Di Cicco⁵

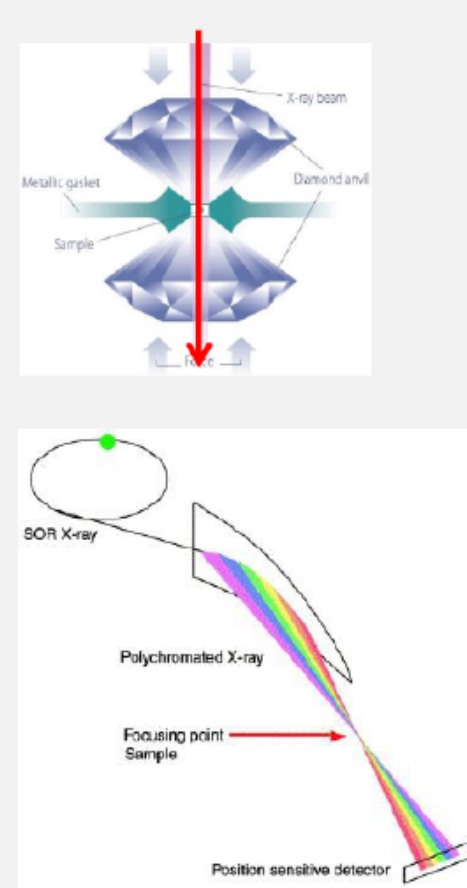
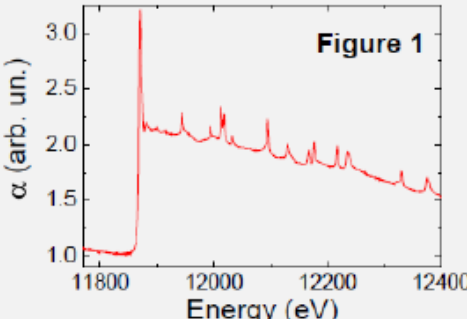
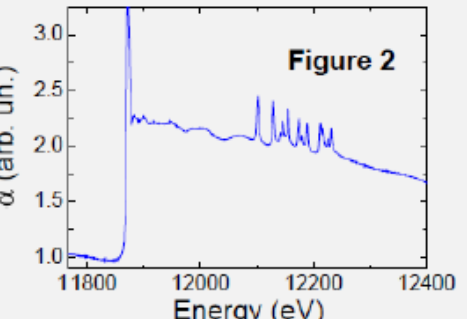
Abstract
X-ray absorption measurements at the L₃ edge of Hg in solid and liquid HgTe have been performed under high-temperature and high-pressure up to 1000 K and 3 GPa using a large volume Paris-Edinburgh press. EXAFS spectra have been analyzed with GNXAS approach. The pressure dependencies of the nearest neighbor distance and the bond variance at room temperature as well as their variation with temperature at 0.6 GPa have been obtained. The temperature dependence of the bond variance has been fitted to the Einstein model and is consistent to the decrease of the bulk modulus with increasing temperature, which has recently been shown to occur by an x-ray diffraction study.

Figure 1: Hg L₃-edge experimental (dots) and calculated (solid line) EXAFS spectra of solid and liquid HgTe at 0.6 GPa as a function of temperature.



The first HP XAS experiment using a PE cell (DCI 1996). Since then, dozens of papers using XAS (and XRD) have been published using this technique.

DAC (dispersive XAS)

Problem solved with nanocrystalline diamonds

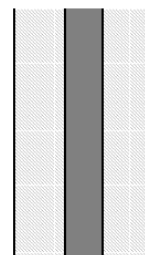
Now possible also at energy-scanning beamlines (microfocus)!

Sample design and combination of x-ray techniques for measuring liquids

Techniques:

- ① X-ray absorption spectroscopy (XAS) → *short-range ordering*
- ② X-ray diffraction (angular, energy-scanning) → *medium and long-range ordering*
- ③ Single-energy XAS → *structure transformation/phase transition detection*

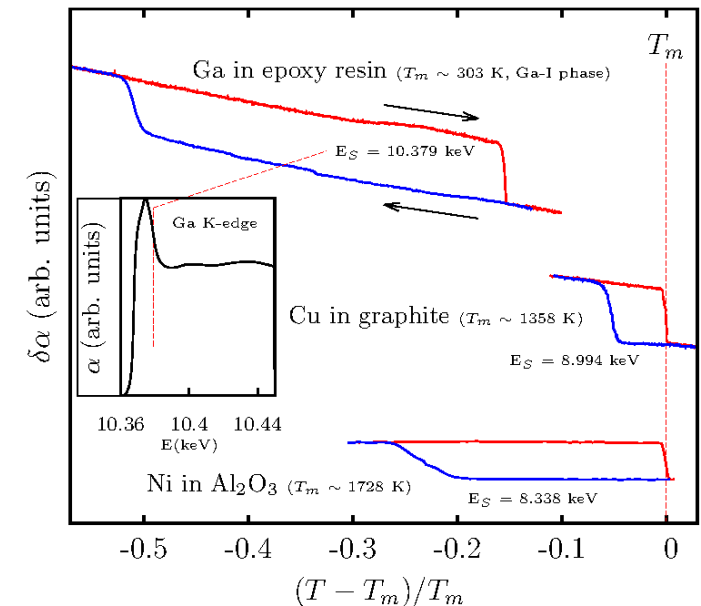
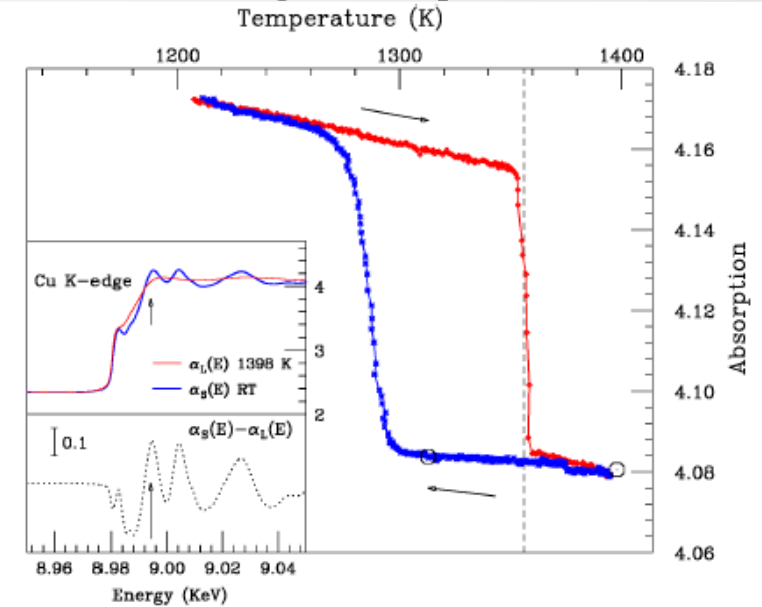
The sample is usually dispersed (b) into a "chemically inert" matrix, low x-ray absorbing and high-temperature resistant (like BN, C, Al_2O_3 , ZrO_2). Micrometric powders of pure materials can be undercooled quite easily hundreds Celsius below the melting point.



(a)

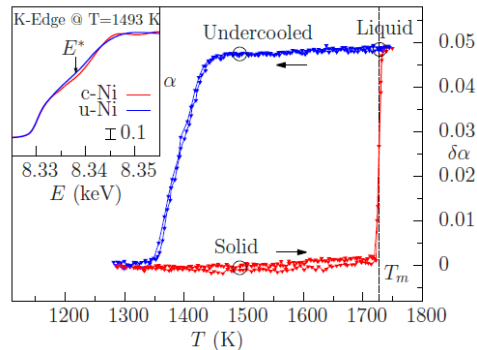


(b)

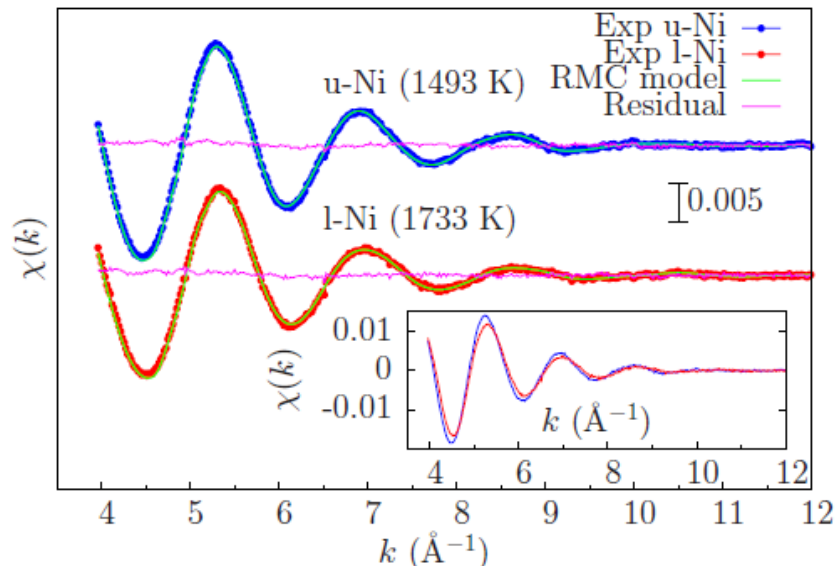


Liquid Ni: unique insight on liquid structure

Pinning liquid and solid phases at high temperature by single-energy Tscan



High-quality EXAFS spectra, differences among liquids at different temperatures



Refs: J. Phys. Condens. Matter 17 S135 (2005), Physical Review B 89, 060102 (2014)

→ Short-range of the liquid reconstructed by accurate multiple-scattering XAS data-analysis.

→ Pair and angular distributions obtained by Reverse Monte Carlo simulations (1372 atoms) using both XRD and XAS data, compared with results of accurate MD simulations

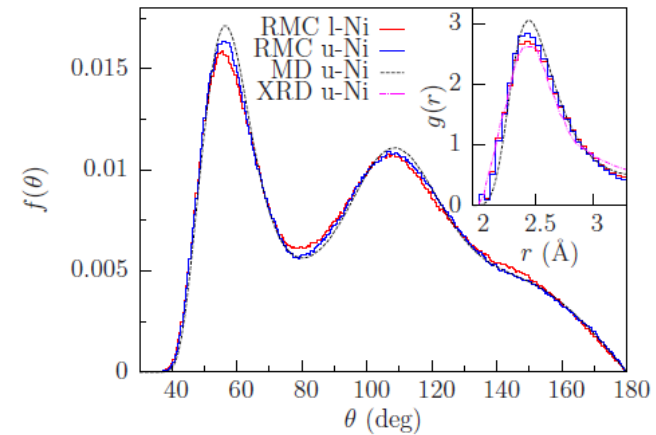


FIG. 3. Normalized bond angle distributions $f(\theta)$ calculated from MD (dashed) and RMC configurations for u-Ni (blue on-line) and l-Ni (red on-line). Inset: first peak of the pair distribution function $g(r)$ obtained by RMC-XAS for l-Ni (red color on-line) and u-Ni (blue color on-line), compared with MD results (dashed) and previous XRD data [19] (dot-dashed).

Local geometry in close-packing liquids

Spherical harmonics invariants

Geometrical characterization of clusters through a set of spherical harmonics invariants (Steinhardt *et al.*, PRB 28, 784 (1982)) calculated for each atom of the simulation at any equilibrium configuration.

$$Q_{lm} \equiv Y_{lm}(\theta(\vec{r}), \phi(\vec{r})) \quad \bar{Q}_{lm} = \frac{1}{N_b} \sum_{\text{bonds}} Q_{lm}(\vec{r}) \quad Q_l \equiv \left[\frac{1}{2l+1} \sum_{m=-l}^l |\bar{Q}_{lm}|^2 \right]^{1/2} \quad W_l \equiv \sum_{m_1+m_2+m_3=0} \begin{bmatrix} l & l & l \\ m_1 & m_2 & m_3 \end{bmatrix} \times \bar{Q}_{l_1 m_1} \bar{Q}_{l_2 m_2} \bar{Q}_{l_3 m_3}$$

TABLE I. Reduced invariants \hat{W}_l , calculated numerically, for the simple shapes whose quadratic and third-order invariants are cataloged in Fig. 2.

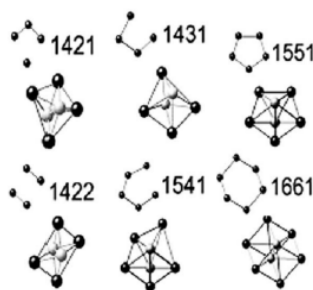
	\hat{W}_4	\hat{W}_6	\hat{W}_8	\hat{W}_{10}
icos		-0.169754		-0.093967
fcc	-0.159316	-0.013161	+0.058454	-0.090128
hcp	+0.134097	-0.012442	+0.051259	-0.079854
bcc	+0.159317	+0.013161	-0.058455	-0.090130
sc	+0.159317	+0.013161	+0.058455	+0.090130

$$\hat{W}_l \equiv \frac{W_l}{\sum_{l=-m}^m [|\bar{Q}_{lm}|^2]^{3/2}}$$

● fcc $\rightarrow \hat{W}_6 = -0.013161$

● icosahedron $\rightarrow \hat{W}_6 = -0.169754$
($\hat{W}_l = 0$ if $l < 6$)

Common neighbor analysis



Different type of pairs are associated with different type of local order

1421 and 1422 - fcc and hcp

1431 and 1541 - defective and distorted icosahedra

1551 - icosahedra

1661 - bcc

RMC-XAS results validated also by MD simulations

		I-Ni (1733 K)	I-Cu (1398 K)	I-Cd (613 K)
1421 + 1422	fcc/hcp	16%	15%	19%
1431 + 1541	def./dis. ico	40%	38%	34%
1551	ico	11%	10%	7%
1661	bcc	3%	3%	2%

Trend of icosahedral ordering in different close-packing liquids probed by XAS: significantly reduced in liquid Cd (hcp with anomalous c/a ratio in the solid phase)

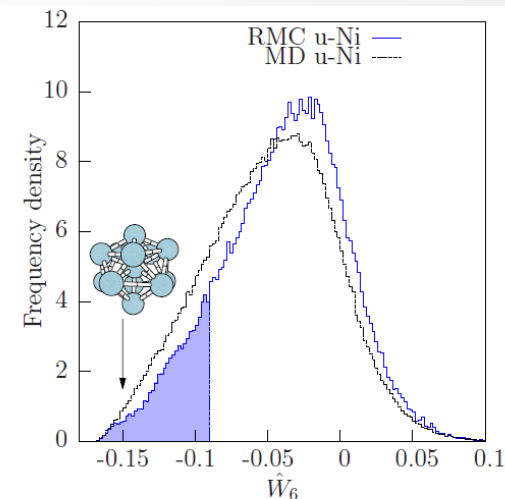


FIG. 5. (Color online) Normalized distribution of the spherical invariant \hat{W}_6 calculated from MD and RMC configurations in u-Ni.

Icosahedral ordering tends to increase in the undercooled phase

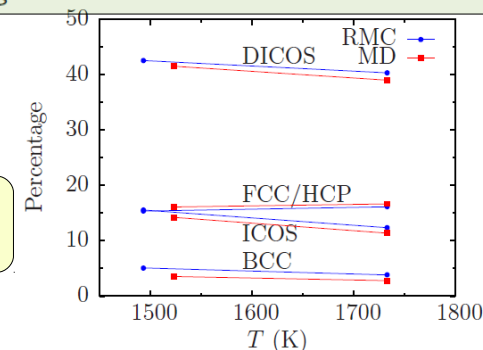


FIG. 4. (Color online) Percentage of nearest-neighbors pairs with given symmetry (CNA analysis of MD and RMC configurations). ICOS, icosahedral (555 pairs); DICOS, distorted icosahedral (544 and 433 pairs); BCC, bcc (666 pairs); and FCC/HCP, fcc and hcp (421 and 422 pairs).

Polymorphism at high pressure: Sn

Polymorphic solid → polymorphic liquid?

Undercooling at high pressure?

Metastable solid states?

Tin, an “easy” example..

Sn-II (diamond structure) ⇒ Sn-I (β -Sn tetragonal structure) ⇒ Sn-III (bct tetragonal)

Polymorphism in the solid phase:

a) phase Sn-II (or α -Sn) (diamond structure) $T < 291$ K - ambient pressure

b) phase Sn-I (or β -Sn) (structure bct(4))

c) phase Sn-III (or γ -Sn) $P > 9.4$ GPa-RT (structure bct(2))

Pressure-induced changes in the liquid:
specific heat, resistivity and TBA signal anomalies associated with possible L-L phase transitions (V. V. Brazhkin et al., High Press. Res. 1997 (267))

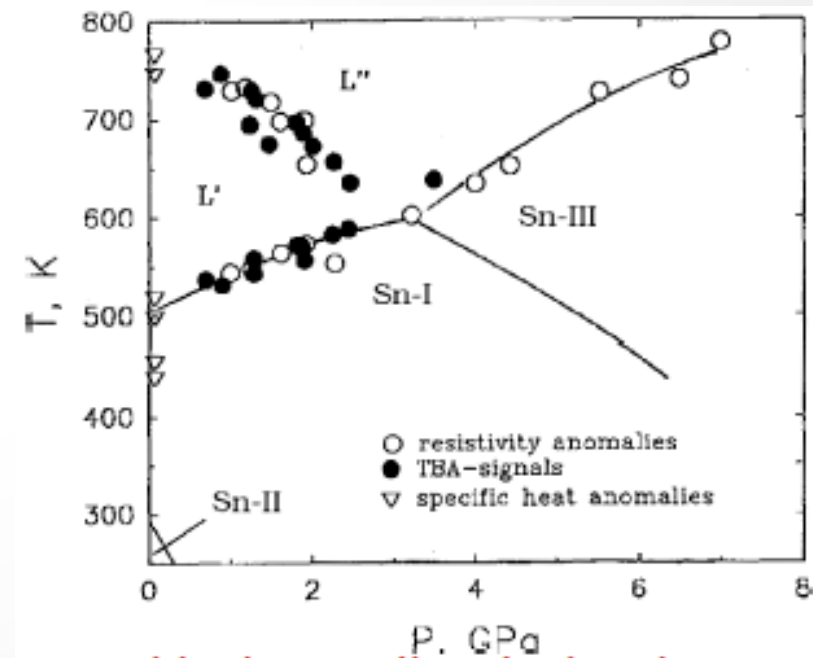
→ differences in the local structure?

XAS/diffraction experiment under HP-HT:

- range of P-T accessible with a large volume press

- access to the undercooled state ⇒ pressure dependence of supercooling (T-scan)

- determination of local structure and symmetries (XAS + RMC)



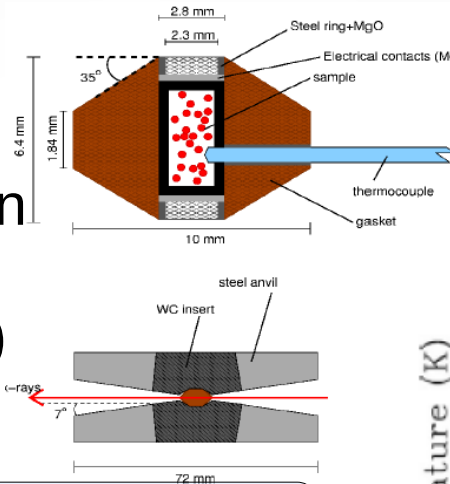
Sn: undercooling and nucleation to metastable phases under pressure

0-9 GPa ÷ 300-1800 K

"large volume" $\approx 1 \text{ mm}^3$

Sn K-edge XAS experiment @ ESRF

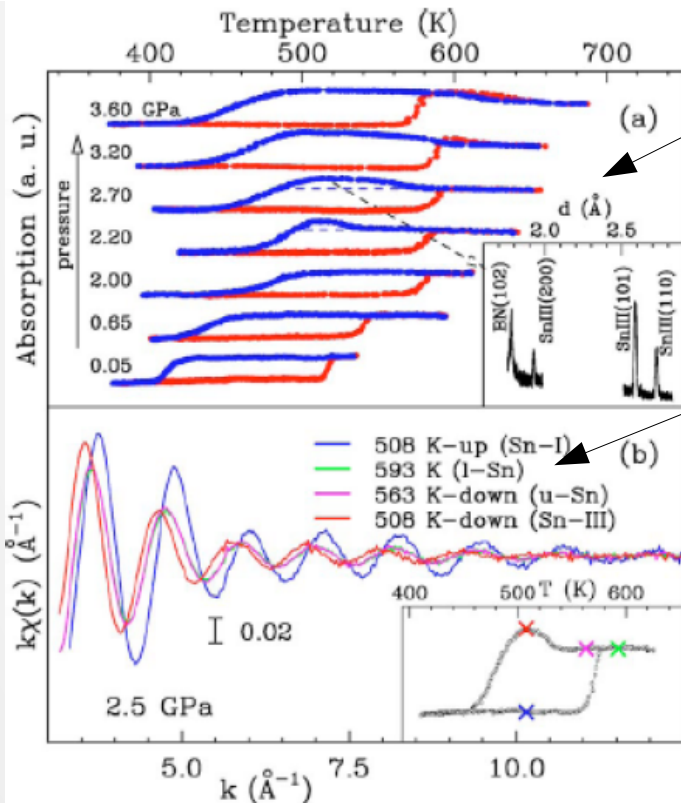
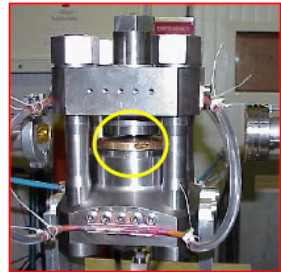
Deep undercooling of Sn submicrometric grains (mixed with LiF and BN)



Mixture with suitable pressure markers (for example LiF)

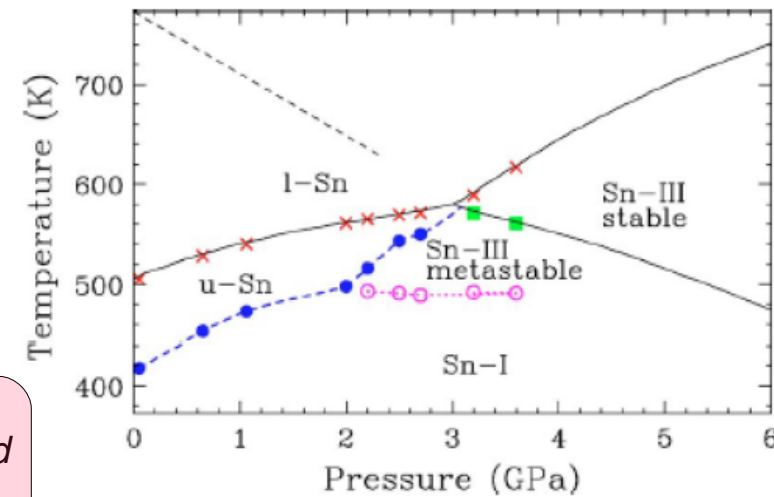
Graphite furnace

Present energy limit $E > 8 \text{ keV}$



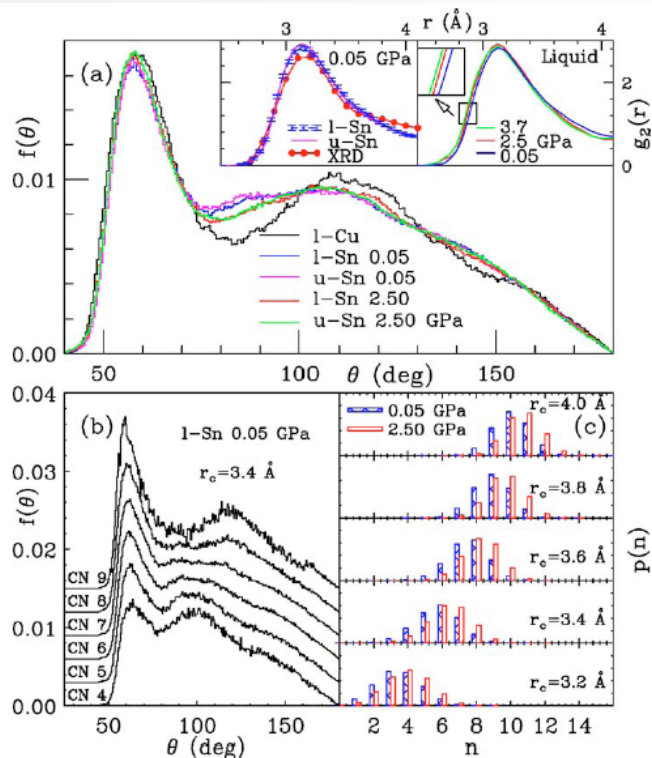
Temperature scans for increasing pressures

XAFS of liquid Sn, undercooled liquid and solid Sn-I and Sn-III are very different!

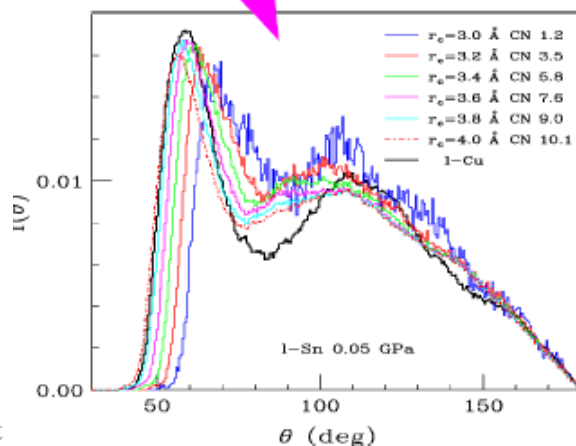


- We observed an abrupt change in the undercooling limit of liquid Sn above 2 Gpa, where nucleation to the Sn-III metastable solid phase take place

Liquid Sn: mixture of tetrahedral and close-packing configurations



- the angular distribution is visibly affected by the cut-off choice
 - $f(\theta)$ is different from that of a “simple” liquid like Cu
 - for lower cut-off increased weight of local configurations with $\theta \approx 100^\circ$
- RMC-XAS



- The liquid local structure is found to be composed of tetrahedral and close-packed configurations.
- The latter confs dominate at high pressure favoring crystallization to the Sn-III metastable solid phase.
- Details in A. D. C. et al., APL **89**, 221912 (2006). Ab-initio MD confirmed the gradual transition from an anisotropic to a nearly close-packed structure under pressure (Munejiri et al., JPCS **98** (2008) 042010)

- Reverse Monte Carlo analysis of XAS data allowed us to reconstruct the short-range pair and three-body distributions.

FIG. 3. (Color online) Panel (a): angular distributions of *l*-Sn and *u*-Sn at 0.05 and 2.5 GPa, where the nucleation of the Sn-III phase takes place. Inset (left): pair distribution functions of *l*-Sn and *u*-Sn compared with the $g(r)$ measured by x-ray diffraction (Ref. 21). Error bars estimated from the RMC modeling are also shown. Inset (right): $g(r)$ of *l*-Sn just above the melting temperature as a function of pressure. Panel (b): normalized angular distributions of liquid Sn at 0.05 GPa calculated around atoms having selected coordination numbers, within a sphere of radius 3.4 Å. Panel (c): probability distribution $p(n)$ of the coordination numbers at 0.05 GPa (blue) and 2.5 GPa (empty red), for different cutoff values. The weight of high-coordinated configurations increases at high pressure.

Polyamorphism of Ge under pressure

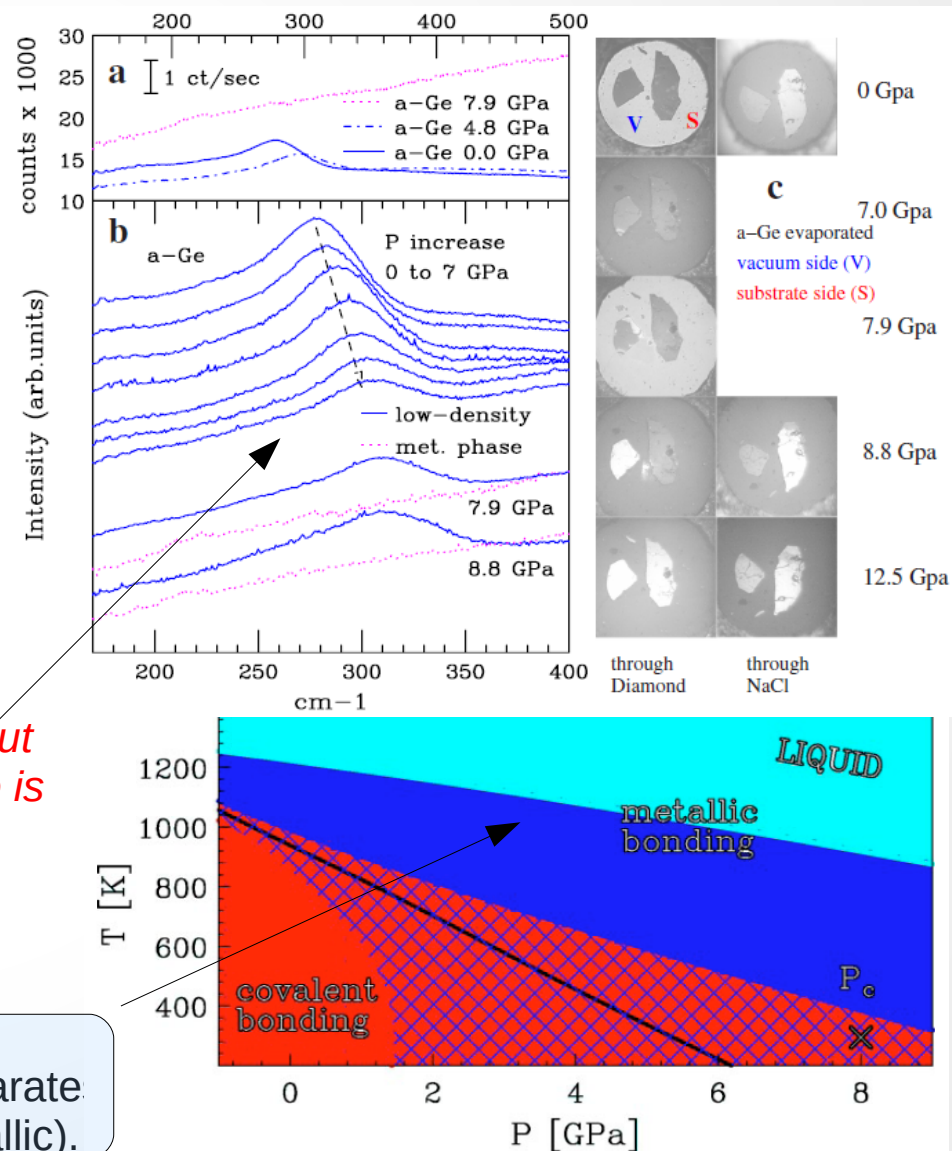
- **Ge/Si polyamorphism: competition between covalent and metallic bonding**

- Evidence of resistivity drop at 6 GPa in a-Ge (Shimomura 1974)
- No clear evidence of transitions up to ~9 GPa by XAS (Freund 1990)
- Evidence of a-Ge crystallization above 6 GPa (Tanaka 1991)
- Evidence of metallization and LDA-HDA transition around 8 GPa by Raman, XAS (A.D.C. et al. 2004, 2008) in a DAC

Interplay between morphology and metallization in amorphous-amorphous transitions
 PHYSICAL REVIEW B 78, 033309 (2008)

Metalization is clearly seen at high pressure by Raman but XAS/XRD is needed to check whether the metallic phase is ordered or disordered. A detailed XRD/XAS study on different beamlines (BM29, ODE, GSCARS) was carried, corroborated also by MD simulations

Hypothetical PT diagram for liquid Ge (2-fluid model). A coexistence line and a metastability region (shaded) separate two liquids: low-density (covalent) and high-density (metallic).



XAS results on amorphous Ge under pressure

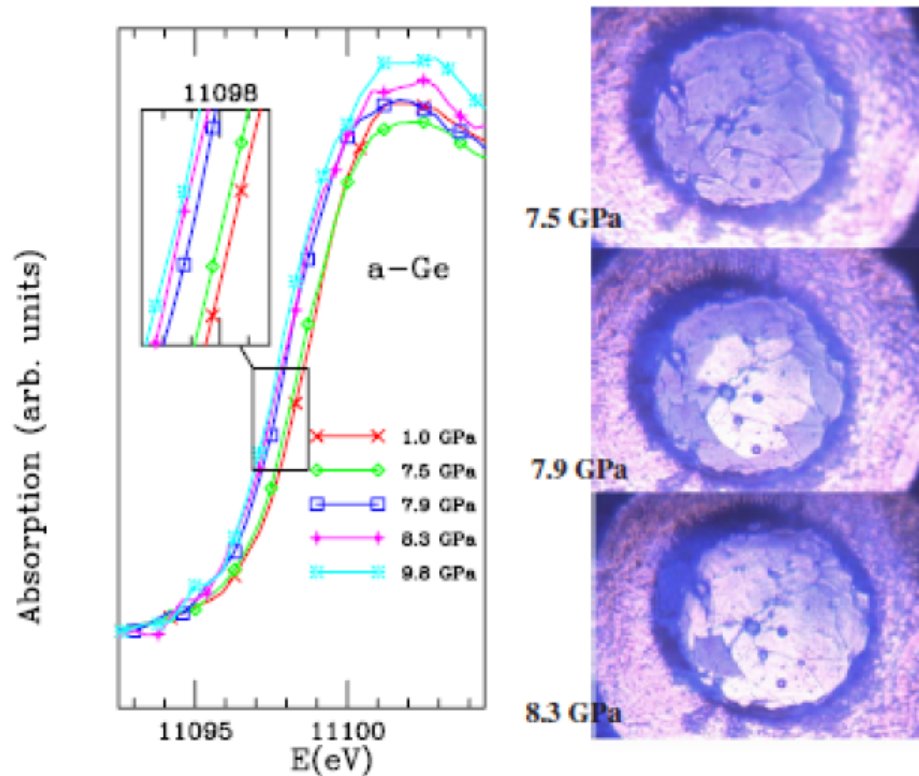


FIG. 3. (Color online) Left panel: shift of the Ge K edge structure at high pressures (all data normalized to 1). The shift to lower energies around 8 GPa is associated with the disappearance of the gap in a metallic state. Right panel: micrographs of the a -Ge sample through the diamonds. The transition to a highly reflective metallic state is clearly visible.

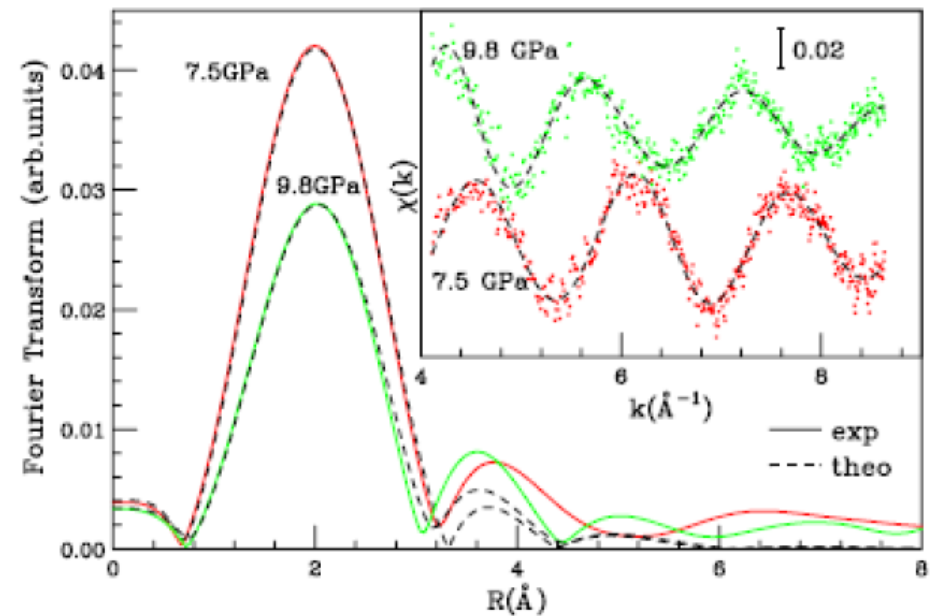


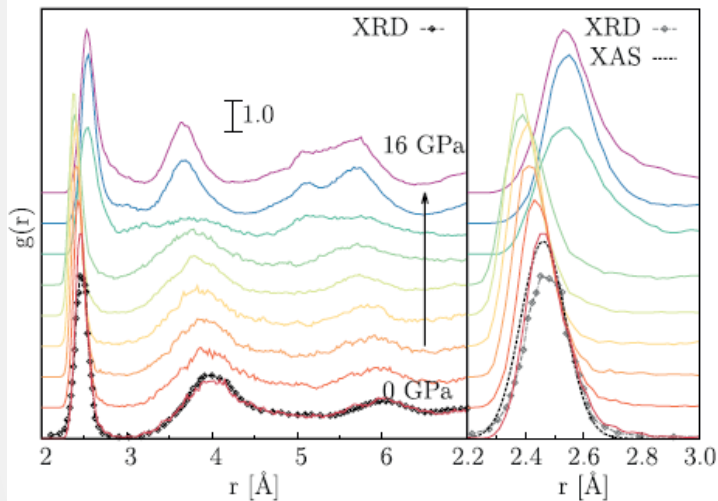
FIG. 8. (Color online) Fourier transforms and XAS signals (inset) of sample before and after the metallization onset (around 8 GPa). Raw XAS spectra and FT patterns are shown as red (7.5 GPa) and green (9.8 GPa) lines (FT) and dots (XAS). Best-fit curves obtained by GNXAS data analysis are shown as dashed black lines.

Data collected at ODE beamline (Soleil) in dispersive mode (combined XAS/XRD)

LDA-HDA transformation in a-Ge

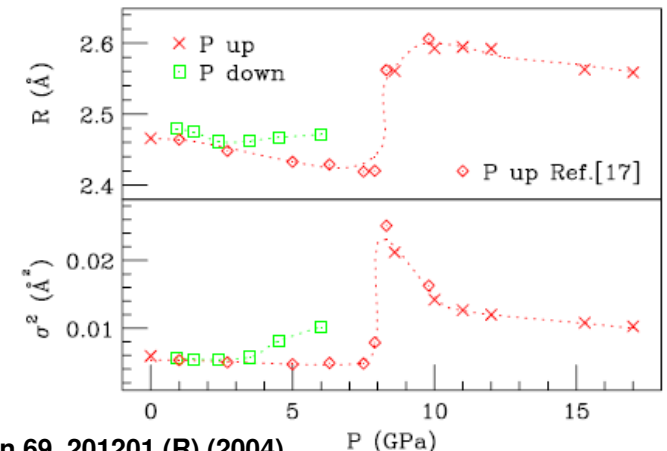
Clear evidence for an increase in average Ge-Ge distance (coordination) and sudden increase of disorder in the region 8-10 GPa.

Sample above 10 GPa is β -Sn and an amorphous structure is recovered upon depressurization at lower pressure



XAS experiments and MD simulations indicates that a low-density to high density transformation (LDA-HDA) occurs around 8 GPa, followed by crystallization above 10 GPa.

HP XAS experiments were carried out both at ODE (Soleil, dispersive mode) and at GSCARS (APS, Argonne, energy-scanning)



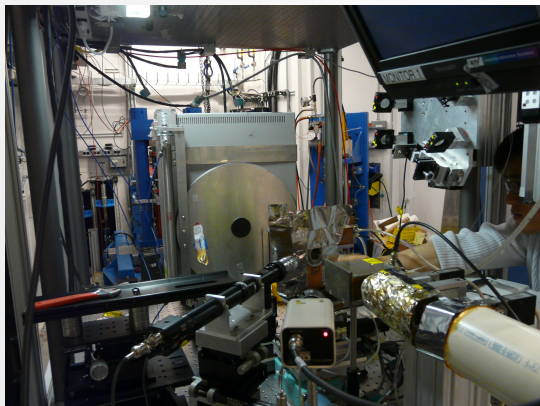
First XAS evidence → **Phys. Rev. B Rapid Communication 69, 201201 (R) (2004)**

Raman + XAS → **Phys. Rev. B 78, 033309 (2008)**

Raman + XAS + simulations/XRD → **Phys. Rev. B 80, 115213 (2009)** + several papers on High Pressure Res.

Ab-initio computer simulations--> **J. Phys.: Condens. Matter 28, 015401 (2016)**

Di Cicco - Krakow XAFS conf. - Jul 2018



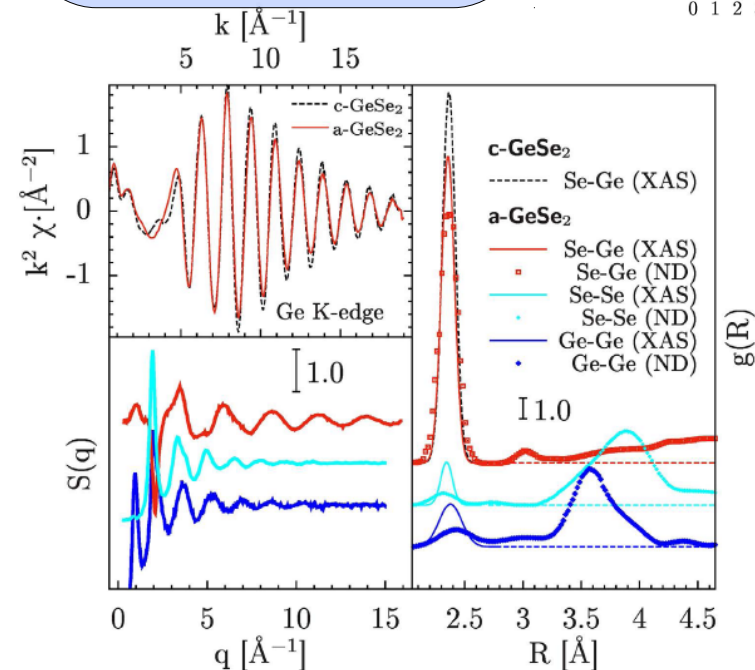
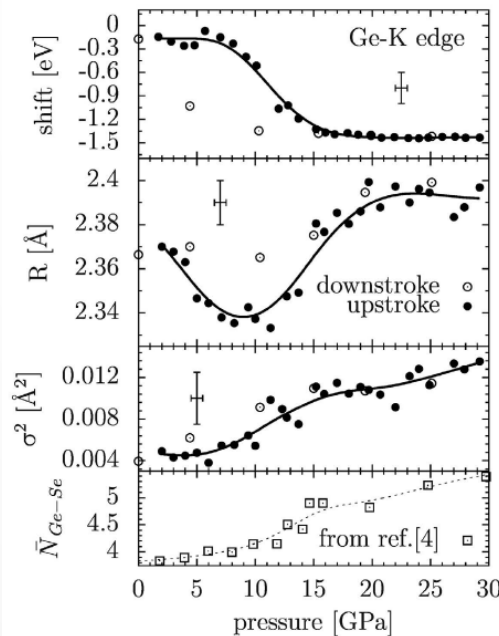
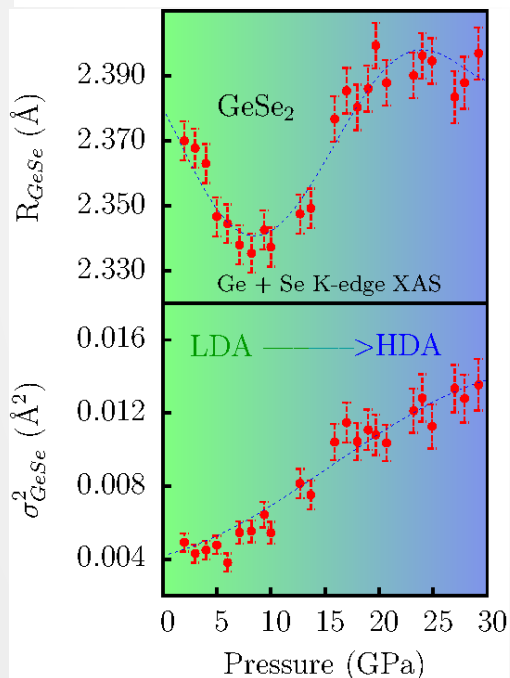
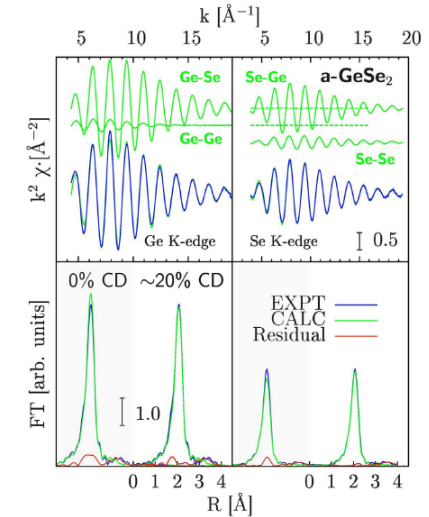
Chalcogenide glasses: LDA-> HDA in GeSe₂

The structure of amorphous GeSe₂ (a-GeSe₂) has been studied by means of a combination of two-edges X-ray absorption spectroscopy (XAS) and angle-dispersive X-ray diffraction under pressures up to about 30 GPa. Multiple-edge XAS data-analysis of a-GeSe₂ at ambient conditions allowed us to reconstruct and compare the first-neighbor distribution function with previous results obtained by neutron diffraction with isotopic substitution. GeSe₂ is found to remain amorphous up to the highest pressures attained, and a reversible 1.5 eV red-shift of the Ge K-edge energy indicating metallization, occurs between 10 GPa and 15 GPa. Two compression stages are identified by XAS structure refinement. First, a decrease of the first-neighbor distances up to about 10 GPa, in the same pressure region of a previously observed breakdown of the intermediate-range order. Second, an increase of the Ge-Se distances, bond disorder, and of the coordination number. This stage is related to a reversible non-isostructural transition involving a gradual conversion from tetra- to octa-hedral geometry which is not yet fully completed at 30 GPa.

L. Properzi^{1,2}, A. Di Cicco¹, L. Nataf², F. Baudalet² & T. Irifune^{3,4}

SCIENTIFIC REPORTS | 5:10188 | DOI: 10.1038/srep10188

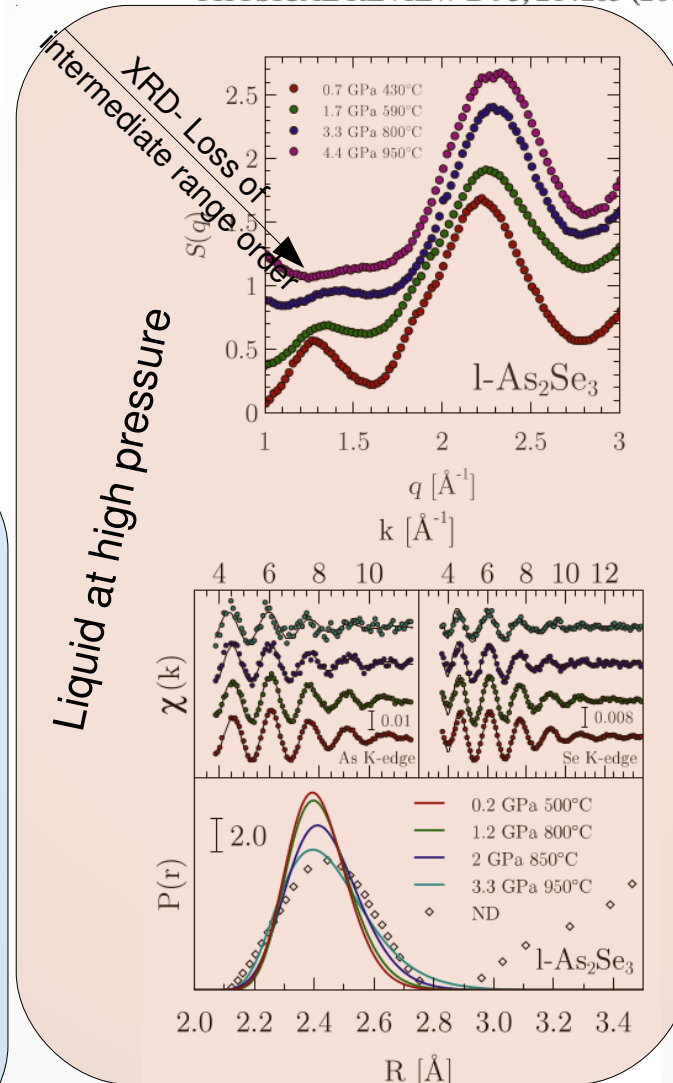
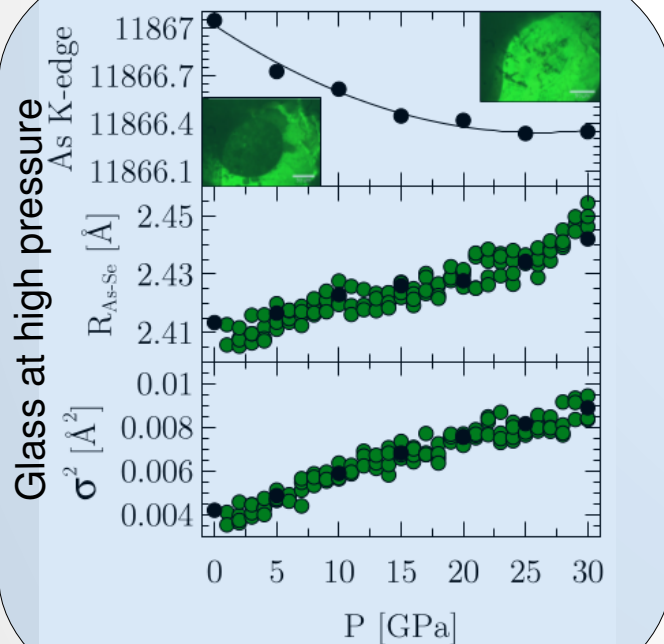
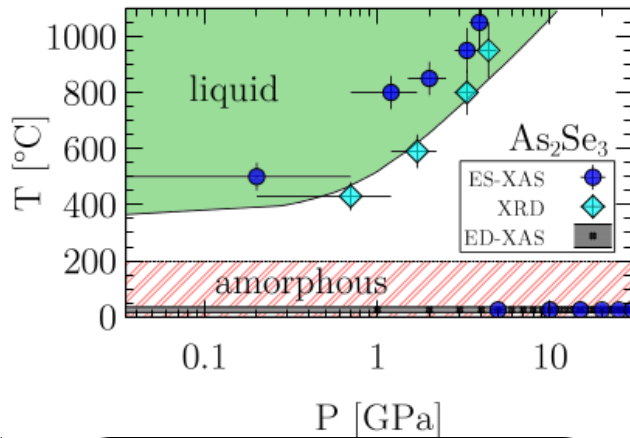
- Metallization 10-15 Gpa
- No crystallization up to 30 GPa
- Increase of average bond distances (around 10 Gpa), variance and coordination number above 10 Gpa
- Transition from tetra to octa-hedral geometry



Chalcogenide glasses: evolution in As_2Se_3

Structural evolution mechanisms of amorphous and liquid As_2Se_3 at high pressures

PHYSICAL REVIEW B 93, 214205 (2016)



- Gradual metallization, evident at 10-15 Gpa
 - No crystallization up to 30 Gpa
 - Continuous increase of As-Se average bond distances, variance
 - No visible changes of coordination numbers (3 for As, 2 for Se), changes involve intermediate order
 - As K-edge is red-shifted, Se K-edge is not → indication of different degrees of delocalization at different atomic sites
- Glass**

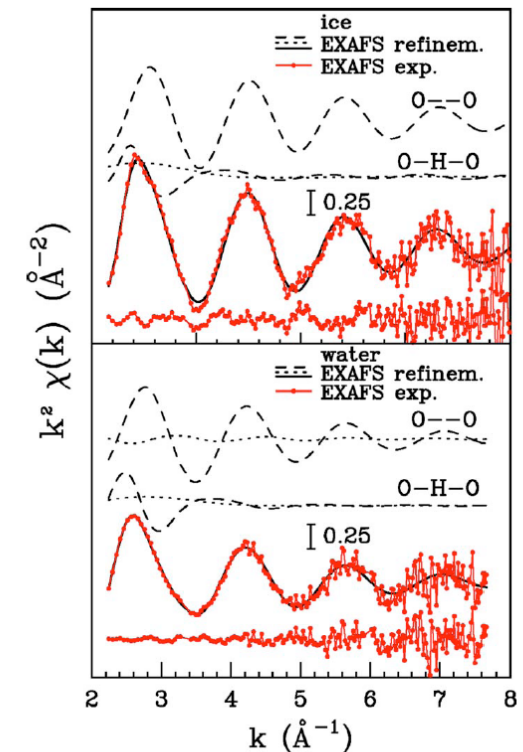
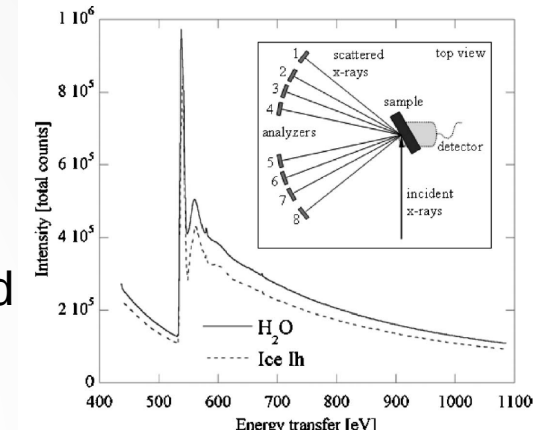
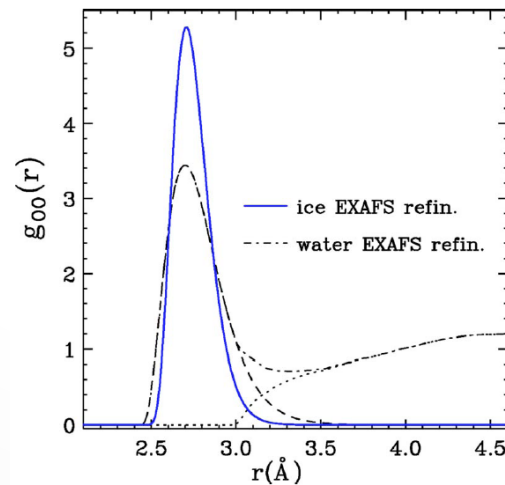
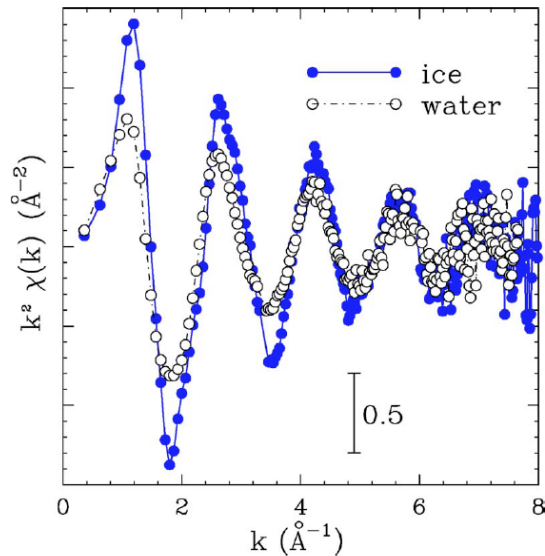
- ➔ Gradual elongation and disordering of As-Se bond distances (XAS)
 - ➔ Asymmetry of the distribution
 - ➔ Loss of intermediate ordering for increasing T, P (XRD)
- Liquid**

A look on “new” developments ...

- XAFS measured by x-ray Raman scattering
- bulk-sensitive XAFS of light elements (like oxygen in water)
- This photon-in photon-out technique (low counting rate) is now readily available (third generation synchrotrons) a
- High-quality XAFS at the O K-edge (543 eV) in water and ice measured at APS (Argonne) at the ID18 undulator beamline (6.9-7.5 keV)

THE JOURNAL OF CHEMICAL PHYSICS 127, 174504 (2007)

Nearest-neighbor oxygen distances in liquid water and ice observed by x-ray Raman based extended x-ray absorption fine structure



Ultrafast XAS at FELs

- Ultrafast XAS measurements at FELs can pump/probe (disordered) matter under extreme/transient conditions
- Several shot-by-shot experiments were performed using hard and soft x-ray at different facilities
- Challenging experiments and new experimental and theoretical problems

PHYSICAL REVIEW B 90, 220303(R) (2014)

Interplay of electron heating and saturable absorption in ultrafast extreme ultraviolet transmission of condensed matter

Al (100 nm) thin film, for EUV radiation and fluence above 1 J/cm² visible deviations due to saturation and electron heating effects are measured

Struct. Dynamics, vol 3. 023604 (2016)

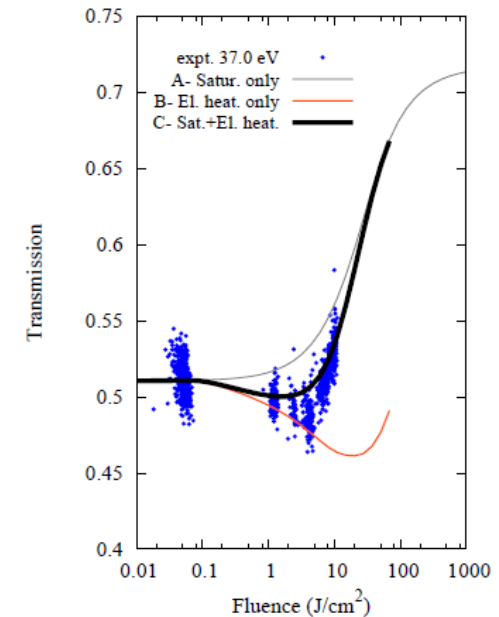
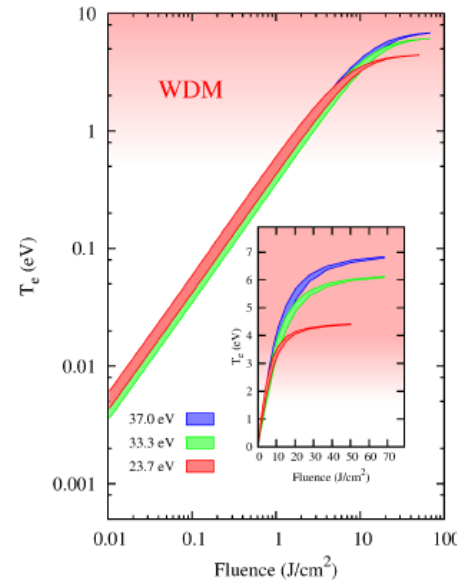
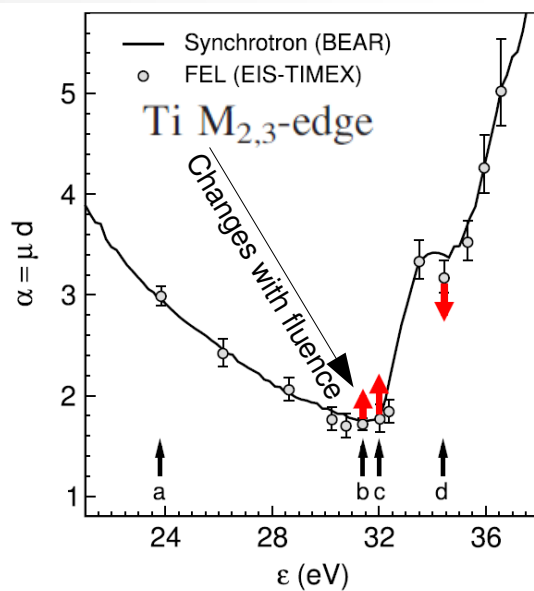


FIG. 3. Experimental EUV transmission data compared with different calculations (see text). Curve A includes only optical saturation phenomena without accounting for temperature effects; curve B includes electron heating but neglects saturation phenomena; curve C takes into account both electron heating and saturation effects.

Acknowledgements

Thanks for your attention!

Collaborators:

- Camerino XAS group (recent): M. Minicucci, A. Trapananti, M. Ciambezi, F. Iesari (now Toyama), L. Properzi (now Firenze), Y. Mijiti, S. J. Rezvani (now Frascati)
- National longstanding collaborations: A. Filipponi (L'Aquila), P. D'Angelo (Roma), G. Aquilanti and L. Olivi (Trieste), C. R. Natoli (Frascati)
- International collaborations: A. Polian (IMPMP Paris), F. Baudelet (Soleil Saclay), K. Hatada (Toyama Univ.), A. Witkowska (Gdansk)